Article

Developmental Cell

Mapping the dynamics of epigenetic adaptation in *S. pombe* during heterochromatin misregulation

Graphical abstract

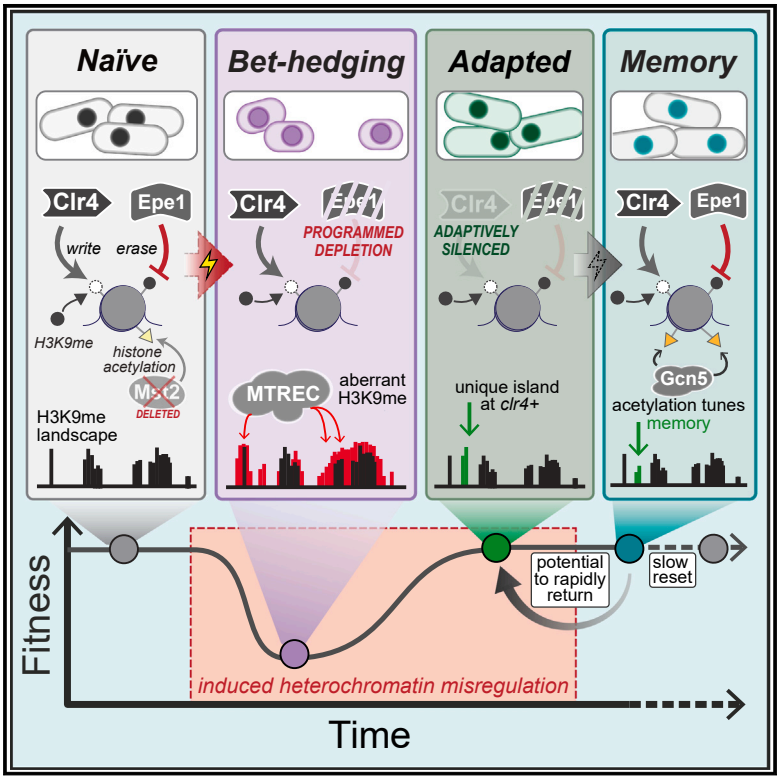

Highlights

- Rapidly induced heterochromatin misregulation leads to slow adaptive *clr4*+ silencing
- Real-time continuous fitness monitoring identifies distinct stress/adaptive phases
- A non-coding RNA-binding complex, MTREC, nucleates stress and adaptive *clr4*+ silencing
- Histone deacetylation tunes the timescale of epigenetic adaptation

Authors

Ajay Larkin, Colin Kunze, Melissa Seman, ..., Sophia Lemieux, Ahmad S. Khalil, Kaushik Ragunathan

Correspondence

khalil@bu.edu (A.S.K.), kaushikr@brandeis.edu (K.R.)

In brief

Larkin et al. develop an inducible system to initiate and reconstruct real-time heterochromatin misregulation dynamics leading to the adaptive silencing of *clr4*+. The MTREC non-coding RNA complex promotes stress-associated H3K9me expansion and nucleates adaptive *clr4*+ silencing, while histone acetylation controls the timescale of epigenetic memory.

Larkin et al., 2024, Developmental Cell *59*, 2222–2238
August 19, 2024
https://doi.org/10.1016/j.devcel.2024.07.006

CellPress

CellPress

Developmental Cell

Article

Mapping the dynamics of epigenetic adaptation in *S. pombe* during heterochromatin misregulation

Ajay Larkin,[1,5] Colin Kunze,[2,3,5] Melissa Seman,[1] Alexander Levashkevich,[1] Justin Curran,[1] Dionysus Morris-Evans,[1] Sophia Lemieux,[1] Ahmad S. Khalil,[2,3,4,*] and Kaushik Ragunathan[1,6,*]

[1]Department of Biology, Brandeis University, Waltham, MA 02453, USA
[2]Biological Design Center, Boston University, Boston, MA 02215, USA
[3]Department of Biomedical Engineering, Boston University, Boston, MA 02215, USA
[4]Wyss Institute for Biologically Inspired Engineering, Harvard University, Boston, MA 02115, USA
[5]These authors contributed equally
[6]Lead contact
*Correspondence: khalil@bu.edu (A.S.K.), kaushikr@brandeis.edu (K.R.)
https://doi.org/10.1016/j.devcel.2024.07.006

SUMMARY

Epigenetic mechanisms enable cells to develop novel adaptive phenotypes without altering their genetic blueprint. Recent studies show histone modifications, such as heterochromatin-defining H3K9 methylation (H3K9me), can be redistributed to establish adaptive phenotypes. We developed a precision-engineered genetic approach to trigger heterochromatin misregulation on-demand in fission yeast. This enabled us to trace genome-scale RNA and H3K9me changes over time in long-term, continuous cultures. Adaptive H3K9me establishes over remarkably slow timescales relative to the initiating stress. We captured dynamic H3K9me redistribution events which depend on an RNA binding complex MTREC, ultimately leading to cells converging on an optimal adaptive solution. Upon stress removal, cells relax to new transcriptional and chromatin states, establishing memory that is tunable and primed for future adaptive epigenetic responses. Collectively, we identify the slow kinetics of epigenetic adaptation that allow cells to discover and heritably encode novel adaptive solutions, with implications for drug resistance and response to infection.

INTRODUCTION

Adaptation enables cells to survive new or changing environments by establishing novel phenotypes that enhance cell fitness.[1,2] These dynamic processes govern how organisms respond to a wide range of physiological contexts, including how cells in our body respond to infections, how cancer cells react to chemotherapeutic agents, and how microbes develop antibiotic and antifungal resistance.[3–5] One major mechanism that cells leverage to acquire new phenotypes is altering their DNA sequence through genetic mutations.[6] Although beneficial mutations in populations are rare, cells that acquire such mutations eventually outcompete those that fail to adapt.[7,8] However, genetic mutations represent an inflexible commitment to a new environment that cannot be reversed following a return to cellular homeostasis.[9,10] Furthermore, it is well known that genetic adaptation to one condition is often associated with a fitness loss in other environments, and hence such changes may represent sub-optimal and terminal solutions amidst fluctuating environments.[11]

Alternatively, through epigenetic adaptation, cells acquire new phenotypes without changing their genetic blueprint.[12] While genetic mutations are irreversible, epigenetic changes can buffer against deleterious mutations without compromising overall fitness of the cell.[11,13] In principle, this strategy offers a dynamic, reversible, and flexible form of adaptation well-suited to rapidly changing environmental conditions, especially when such conditions persist only for a few generations.[14–16] Moreover, due to the flexibility of this mode of adaptation, epigenetic changes often pose serious clinical challenges during the evolution of chemotherapy resistance in cancer cells or the widespread emergence of antifungal resistance.[17–21] Thus, understanding how cells leverage adaptive epigenetic mechanisms and targeting such pathways can help us achieve improved clinical outcomes.

In one striking example of heritable and reversible epigenetic adaptation, the yeast translation-termination factor Sup35 can self-aggregate under stress to form the [*PSI*$^+$] prion.[22,23] [*PSI*$^+$] sequesters soluble (active) Sup35, promoting genome-wide translation readthrough, and uncovering previously cryptic genetic variation. The aggregated conformational state, when activated, rapidly unlocks novel and heritable phenotypes that may be beneficial in unanticipated conditions. How can other epigenetic pathways similarly unleash latent, heritable, and adaptive phenotypes?

Considerable evidence suggests that cells can alter their transcriptomes in response to stress through alterations in chromatin accessibility, rewiring existing regulatory networks, and orchestrating wholesale changes in histone modification states.[18,24–30] Moreover, recent work has shown that diverse

histone modifications with different canonical functions may have adaptive potential by being dynamically redistributed to new genomic loci under different stress conditions.[19–21] How cells exploit these heritable, chromatin-based epigenetic programs to discover genes that can be activated or repressed to enhance fitness and survival remains mysterious.

In principle, the adaptive and dynamic redistribution of histone modifications should meet three critical requirements. First, modifications can spatially redistribute, either through spreading from existing sites or the formation of new islands at novel locations in the genome. This allows cells to sample altered chromatin and transcriptional states. Next, the resulting histone modification-dependent changes in gene expression must benefit cells and their progeny in this new environment.[31] This enables cells that identify optimal adaptive solutions to persist and become dominant in the population. Lastly, memory of the new cell state can prepare cells to more rapidly respond to a future instance of being exposed to the initiating stress.[32–36] Thus, to faithfully map epigenetic adaptation pathways, it is necessary to reconstruct these highly dynamic processes and be able to connect genome-wide changes at the RNA and chromatin levels with cell fitness prior to and following adaptation.

To reconstruct these dynamics, we developed an experimental system based on the fission yeast, *Schizosaccharomyces pombe* (*S. pombe*). In *S. pombe*, H3K9 methylation (H3K9me) specifies silent epigenetic states otherwise referred to as heterochromatin.[37] Although heterochromatin normally resides at regulatory regions of the genome, such as centromeres and telomeres, H3K9me can also be deployed to downregulate novel targets.[38–46] One example of an acute stress in *S. pombe* that elicits an adaptive epigenetic response is so-called ''heterochromatin misregulation.'' Deleting two major H3K9me antagonists—the H3K14 histone acetyltransferase Mst2 and the putative H3K9 demethylase Epe1—leads to the adaptive silencing of the sole H3K9 methyltransferase, Clr4, suppressing aberrant genome-wide H3K9me and restoring fitness.[47] We reasoned that this system would provide an ideal, minimal, and genetically pliable framework to induce heterochromatin misregulation and unveil the sequence of events that occur prior to adaptation.

We developed a precision genetic approach to trigger and reverse heterochromatin misregulation on-demand.[48,49] Taking inspiration from laboratory evolution experiments, which have been powerful in defining genetic adaptations in microbial populations grown under selective pressure, we coupled this ability to induce heterochromatin misregulation with advanced continuous culture methods that allow us to quantify cell fitness in real-time and identify causal genome-wide transcriptional and chromatin-state changes.[50] Our inducible experimental system is a significant departure from previous studies that focused primarily on beginning and end-state measurements.[21] By quantifying cell fitness in yeast populations, we could precisely trace the time evolution of the adaptive silencing program under multiple cycles of heterochromatin stress and recovery. Our approach uncovers how cells can redistribute H3K9me, records network-level changes in transcription, and defines how this dynamic interplay unlocks cryptic epigenetic variation to enable cell survival under conditions of acute stress. In summary, our study captures key features of how cells turn an existing regulatory pathway that normally ensures H3K9me is deposited only at constitutive sites into an adaptive mechanism with implications for drug resistance and response to infection.

RESULTS

An inducible Epe1 depletion system to trigger heterochromatin misregulation on-demand

Epe1, a putative H3K9 demethylase, and Mst2, an H3K14 acetyltransferase, have additive roles in regulating *S. pombe* heterochromatin. Deleting both Epe1 and Mst2 leads to acute heterochromatin misregulation, promoting an adaptive epigenetic response.[47] We first confirmed previously published results by generating *mst2Δepe1Δ* cells, which successfully adapted by silencing the H3K9 methyltransferase, Clr4. We measured an approximately ~4-fold decrease in Clr4 mRNA levels and the establishment of adaptive H3K9me2 at the *clr4+* locus (Figures S1A–S1C).

We designed a system to trigger heterochromatin misregulation on-demand by inducibly, rapidly, and completely depleting Epe1. This enables us to induce acute heterochromatin misregulation and subsequently trace the ensuing adaptive response circumventing the limitations associated with endpoint genetic measurements. Our system controls Epe1 at (1) the transcriptional level, through the thiamine-repressible promoter (*nmt81*), and (2) the protein level, by fusing an auxin-inducible degron tag to the C terminus of Epe1 to trigger ubiquitination-mediated degradation. We refer to this inducibly degradable Epe1 allele as *epe1^{deg}* (Figure 1A).[48,49] Thiamine addition caused an 8-fold reduction in Epe1 mRNA levels which, when combined with napthaleneacetic acid (NAA) supplementation, led to the absence of any detectable Epe1 protein within 30 min (Figures 1B and 1C). Thus, *epe1^{deg}* leads to rapid and negligible protein and transcript levels after addition of NAA and thiamine to cells.

We quantified the mean and standard deviation for colony sizes grown with and without Epe1 (Figure 1D). We observed generally smaller colonies and substantial colony size heterogeneity when we depleted Epe1 in an *mst2Δ* background, reflecting a fitness loss associated with stress (Figures 1D and 1E). Furthermore, *mst2Δepe1^{deg}* cells exhibited a 4-fold decrease in Clr4 mRNA levels after 5 days of Epe1 depletion, recapitulating the adaptation we noted in *mst2Δepe1Δ* cells (Figures 1F and S1C). By contrast, depleting Epe1 in an *mst2+* background caused a less-pronounced growth defect and no detectable adaptive Clr4 silencing, consistent with previous studies.[47]

To test if adaptation was dependent on the order in which the two heterochromatin regulators were depleted, we developed a strain to deplete Mst2 (*mst2^{deg}*) in an *epe1Δ* background (Figures S1D–S1G). While there was still some decrease in colony size upon Mst2 depletion, this strain did not produce the same degree of heterogeneity in colony size (Figures S1E and S1F). Additionally, we observed that Clr4 was silenced to a lesser degree compared with *mst2Δepe1^{deg}* cells (Figure S1G). We also developed strains where both Mst2 and Epe1 could be simultaneously depleted in an inducible manner (*mst2^{deg} epe1^{deg}*), which allowed us to test whether pre-deleting Epe1 or Mst2 produces differences in adaptive phenotypes

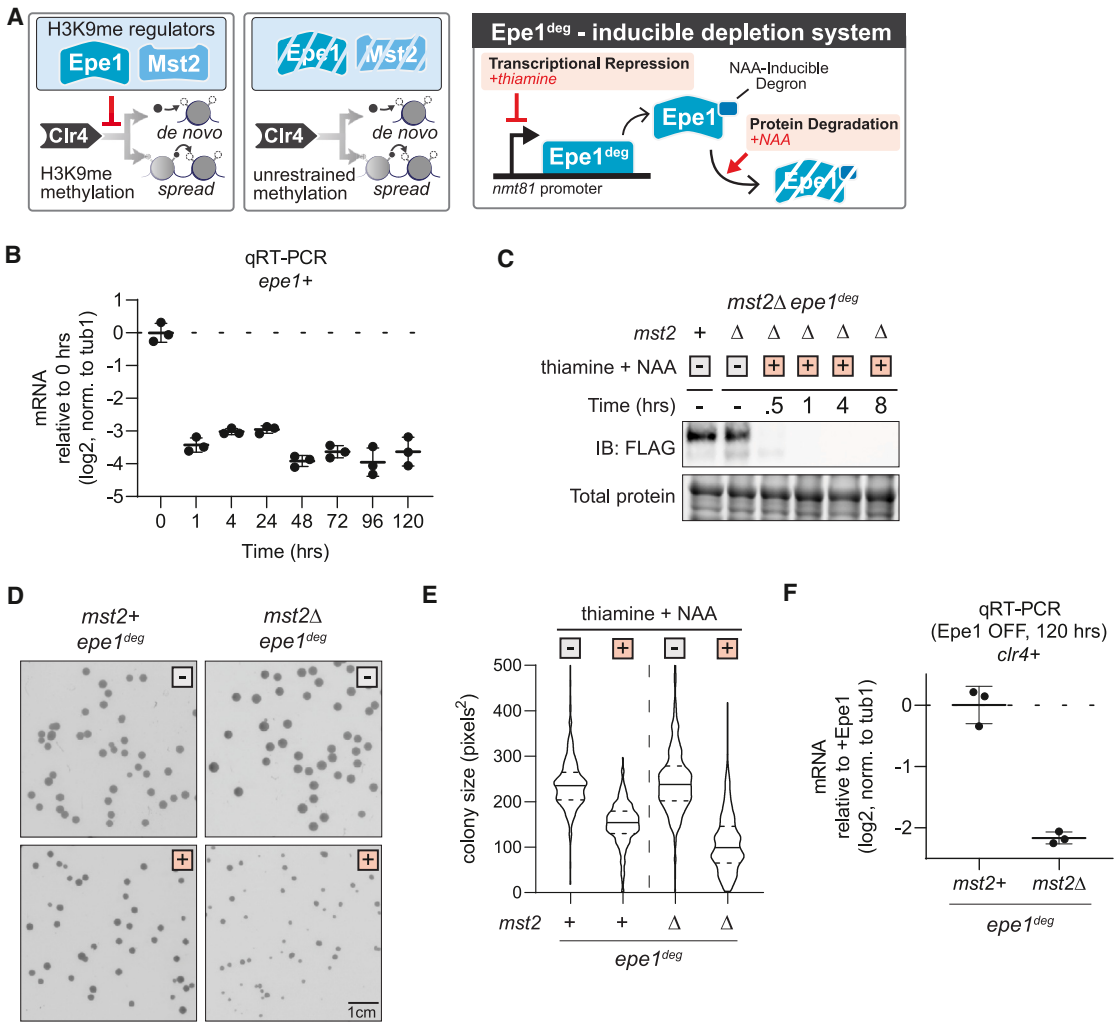

Figure 1. An inducible Epe1 depletion system to trigger heterochromatin misregulation on-demand

(A) (Left) Epe1 and Mst2 prevent uncontrolled H3K9me spreading. The absence of Mst2 and Epe1 triggers heterochromatin misregulation. (Right) Construction of a precision-engineered genetic approach to toggle Epe1 availability in cells (Epe1^{deg}). Epe1 transcription is regulated by a thiamine inducible nmt81 promoter, and protein levels are regulated by an auxin-inducible degron tag (AID). Adding auxin and thiamine promotes the on-demand, inducible depletion of Epe1.

(B) RT-qPCR measuring *epe1+* RNA levels following Epe1 depletion, relative to +Epe1. $n = 3$.

(C) Western blot for Epe1-3xFLAG-AID in Epe1^{deg} strains.

(D) *S. pombe* colonies on solid media after 3 days of growth.

(E) Colony size distribution in indicated genetic backgrounds and growth conditions, quantified after 5 days of growth. Mean and standard deviation of distributions in pixels^2: *mst2 + epe1^{deg}* no treatment (240.4 ± 64.2), thiamine and NAA (151.2 ± 46.6); *mst2Δepe1^{deg}* no treatment (246.2 ± 74.6), thiamine and NAA (109.4 ± 64.0).

(F) RT-qPCR measuring *clr4+* RNA levels following 5 days of Epe1 depletion, relative to +Epe1. $n = 3$.

Depletion is pictorially indicated with either a white box for no treatment or an orange box for treatment. Error bars represent standard deviation.

(Figure S1H). *mst2^{deg}epe1^{deg}* exhibited comparable levels of colony size variegation and more robust *clr4+* mRNA suppression compared with *mst2Δepe1^{deg}* (compare Figures 1C–1E to Figures S1I–S1K). Nevertheless, we noted residual levels of Mst2 protein in *mst2^{deg}* strains that remained refractory to depletion, which we reasoned could potentially have unintended consequences on our adaptation measurements (Figures S1D and S1H). Collectively, our results establish a system for the inducible, rapid, and complete depletion of Epe1 and demonstrate that the *epe1^{deg}* allele recapitulates how *S. pombe* cells adapt in response to acute heterochromatin misregulation.[47]

Time evolution of adaptive silencing during heterochromatin misregulation

To trace adaptation following Epe1 depletion, we deployed the automated eVOLVER continuous culture platform (Figure 2A).[51,52] eVOLVER enables long-term maintenance of independent *S. pombe* cultures in miniature bioreactors using a continuous turbidostat routine with real-time growth rate quantification.[53–55] The eVOLVER system also features the ability to schedule media changes, including switching between non-inducer and inducer media. As a result, we can precisely quantify changes in growth resulting from Epe1 depletion and sample

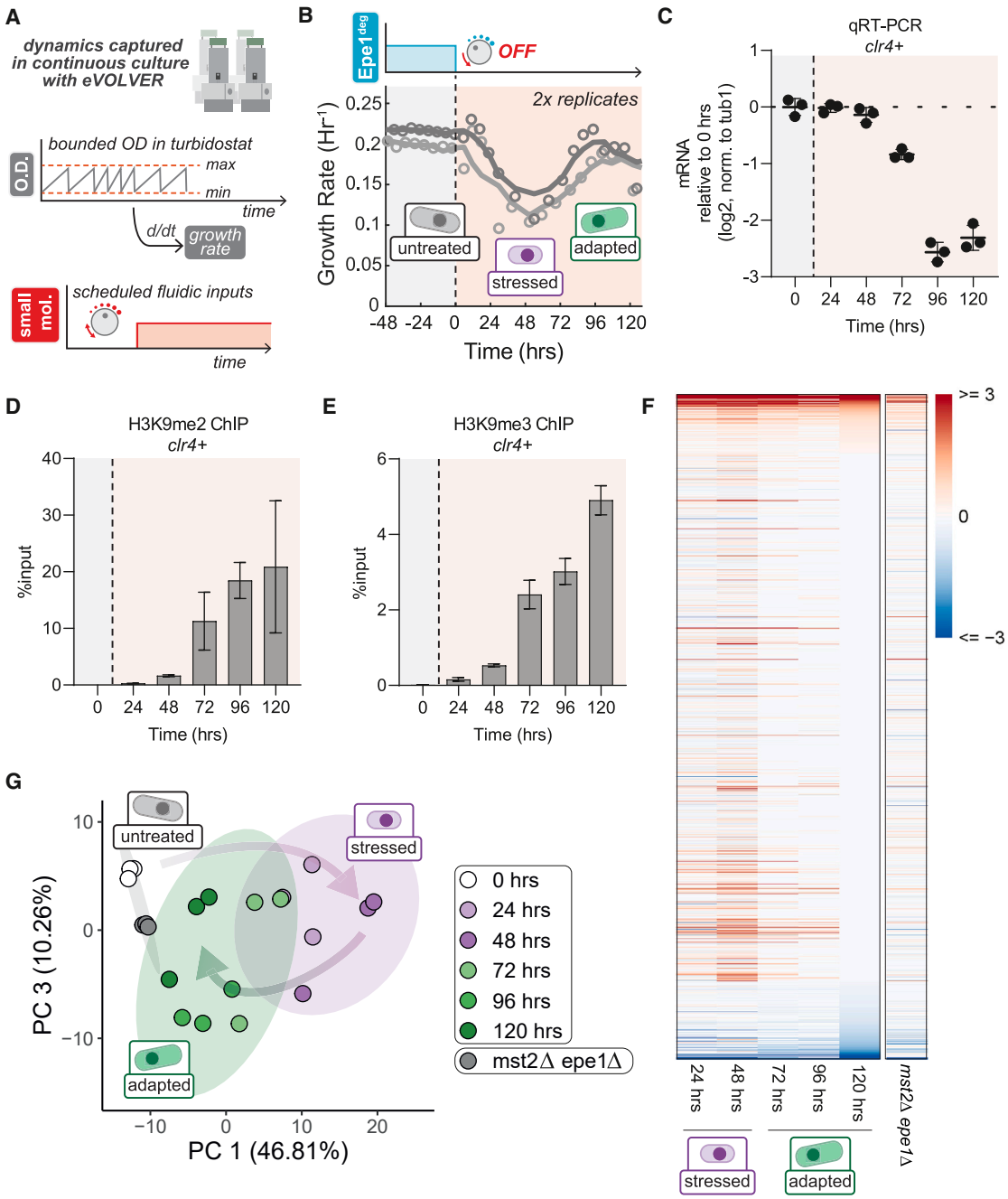

Figure 2. Time evolution of adaptive silencing during heterochromatin misregulation

(A) We used the eVOLVER system to control growth of cells using a continuous turbidostat routine, with real-time quantification of growth rate and scheduled media changes.

(B) Real-time monitoring of *mst2Δepe1*^{deg} growth rates in eVOLVER. Lines represent moving averages. Epe1 depletion was initiated at t = 0 h. Individual trendlines indicate replicates (N = 2).

(C) RT-qPCR measuring *clr4+* RNA levels following 5 days of Epe1 depletion, relative to +Epe1. n = 3.

(D) H3K9me2 ChIP-qPCR measured at the *clr4+* locus as a function of time following Epe1 depletion. n = 2.

(E) H3K9me3 ChIP-qPCR measured at the *clr4+* locus as a function of time following Epe1 depletion. n = 2.

(F) Heatmap of significant differentially expressed genes following Epe1 depletion relative to untreated cells. Transcripts shown n = 3,896, significance cutoff of Adj$p$val $\leq$ 0.01.

(G) PCA of indicated RNA-seq samples. n = 3, ellipse level = 0.9.

Orange shaded portion represents the Epe1 depletion period. Error bars represent standard deviation.

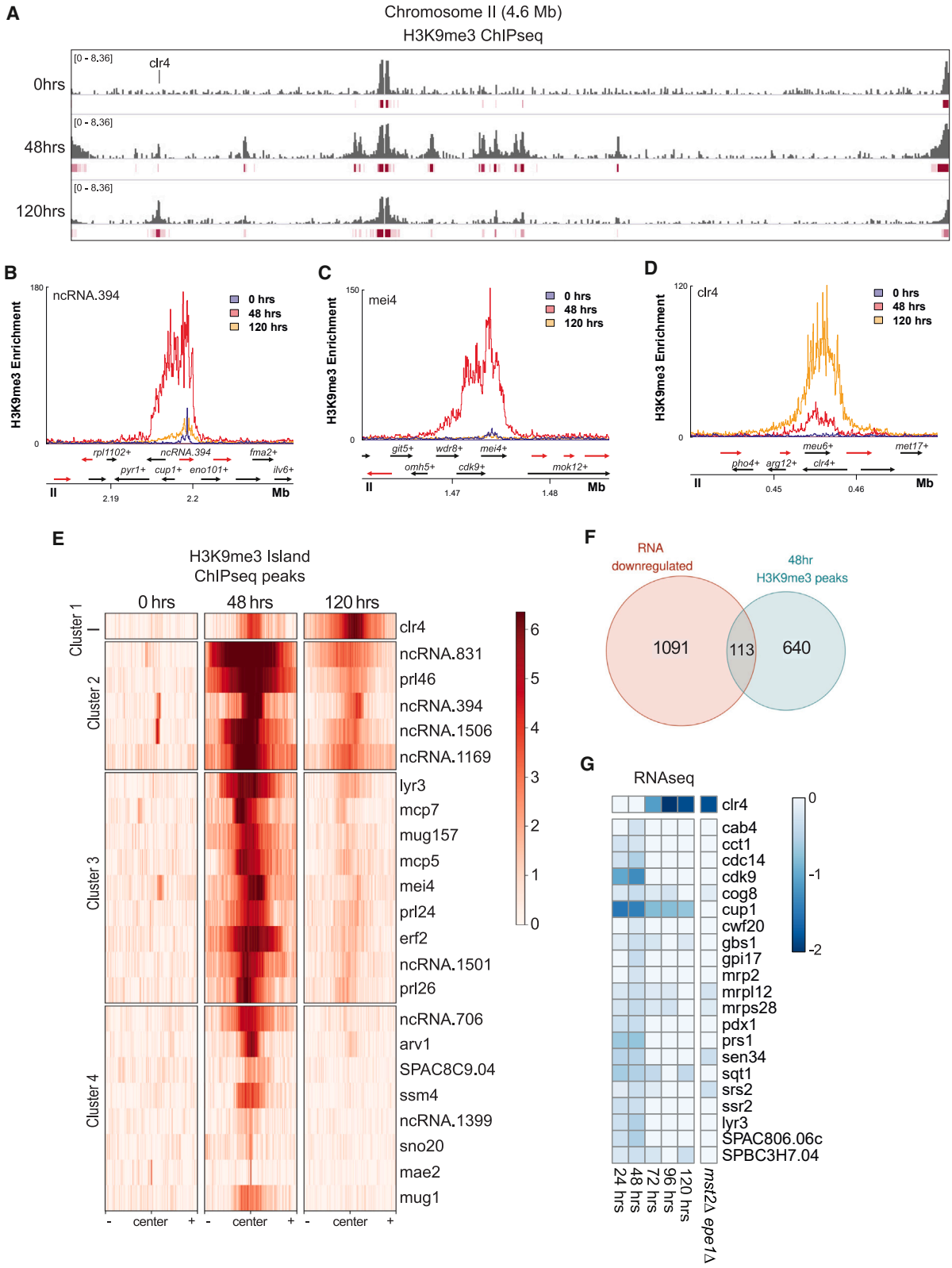

Figure 3. Heterochromatin misregulation triggers the targeted expansion of pre-existing H3K9me3 islands

(A) H3K9me3 ChIP-seq over *S. pombe* chromosome II. Enrichment is in $\log_2$ fold change of immunoprecipitation (IP) normalized to input. Time of Epe1 depletion is indicated on the left side of each track. Peaks identified are denoted in red below each track.

(legend continued on next page)

cells as a function of time for molecular measurements to reconstruct the dynamics of Clr4 silencing and concomitant changes in transcription.

We grew *mst2Δepe1*^{deg} populations in eVOLVER for 48 h at 32°C before switching to inducer media to trigger Epe1 depletion (STAR Methods). Upon induction, we observed a substantial growth rate reduction over 48 h, followed by growth recovery corresponding to successful adaptation (Figure 2B). Based on the eVOLVER time traces, we posited that cells transit through three primary phases upon experiencing heterochromatin misregulation: (1) untreated (before inducing Epe1 depletion) (2), stress (post-induction, characterized by poor growth), and (3) adapted (growth recovery). Replicate eVOLVER populations of *mst2*^{deg}*epe1*^{deg} closely followed these same growth trends (Figure S2A). By contrast, we observed little change in the growth rate in *mst2Δepe1*^{deg}*clr4Δ* populations upon induction of Epe1 depletion, supporting that the growth rate changes in *mst2Δepe1*^{deg} strains were dependent on H3K9me (Figure S2B).

We then harvested *mst2Δepe1*^{deg} cells grown in 24-h time intervals for quantification of *clr4*+ mRNA and H3K9me2/me3 levels. In the initial stress phase (during the first 48 h post-induction), we observed no changes in *clr4*+ mRNA and very minimal increases to H3K9me2/me3 levels (Figures 2C–2E). However, after 48 h, we observed a substantial decrease in *clr4*+ mRNA expression, coinciding with H3K9me2/3 enrichment (Figures 2C–2E and S2C–S2D). Thus, the transition between the stress and adapted phases is closely aligned with Clr4 repression. These results demonstrate that growth rate and Clr4 silencing dynamics are closely coordinated as cells respond to stress arising from heterochromatin misregulation.

To assess transcriptome-wide changes during Epe1 depletion, we performed RNA sequencing (RNA-seq) on *mst2Δepe1*^{deg} samples, collected at 24-h intervals. In the stress phase, we observed acute changes to the transcriptome relative to untreated *mst2Δepe1*^{deg} cells (Figure 2F). Principal-component analysis (PCA) clearly captured time-dependent transitions between different growth phases following Epe1 depletion, showing these gene expression changes gradually vanished by the time adaptation was completed (Figures 2G and S2E).

We additionally performed RNA-seq analysis on *mst2Δepe1Δ* cells to compare with *mst2Δepe1*^{deg} cells. Most strikingly, the transcriptomes of these cells most closely resembled untreated *mst2Δepe1*^{deg} cells (0 h) (Figures 2G and S2E). Importantly, independent *mst2Δepe1Δ* clones have few differences in their transcriptomes, implying that different isolates make similar adaptive choices (Figures S2F and S2G). Since *mst2Δepe1Δ* silences *clr4*+ and has been grown well beyond 120 h, their convergence toward the untreated transcriptome implies that there are additional RNA level changes that occur beyond our 120-h adaptation time course. For example, we found that, in Epe1-depleted cells at 120 h, genes associated with iron homeostasis are upregulated while genes associated with ATP synthesis and cellular respiration are downregulated (Figure S2H; Table S4). In *mst2Δepe1Δ* cells, these genes returned to expression levels equivalent to untreated *mst2Δepe1*^{deg} cells (Figure S2I).[39] Taken together, our system reveals distinct population-level cell states during the adaptation process.

Heterochromatin misregulation triggers the targeted expansion of pre-existing H3K9me3 islands

To investigate how heterochromatin misregulation drives changes in the H3K9 methylome over time, we grew *mst2Δepe1*^{deg} batch cultures over 120 h. chromatin immunoprecipitation sequencing (ChIP-seq) revealed expansion of specific heterochromatin domains, with very little enrichment for H3K9me3 peaks outside these regions. These domains were primarily at constitutive heterochromatin (pericentromeres, telomeres, and the ribosomal DNA locus) and several heterochromatin islands centered around meiotic genes and ncRNAs (Figures 3A and S3A; Table S5).[46,47,56] We clustered H3K9me3 island peaks into four groups, where three clusters show a pattern of H3K9me3 spreading up to the end of stress phase (48 h) followed by a steady decay of H3K9me3 in the adapted phase (Figures 3B and 3C). In contrast to other islands, H3K9me3 is deposited *de novo* at the *clr4*+ locus and accumulates over time (Figures 3D, 3E, and S3B). Subsequent ChIP-seq in *mst2*^{deg}*epe1*^{deg} also confirmed that pre-deletion of Mst2 does not drive pre-adaptation, wherein the islands that expand during adaptation are identical to *mst2Δepe1*^{deg} cells (Figures S4A and S4B).

We cross-referenced our H3K9me3 ChIP-seq and RNA-seq time course data to measure transcriptomic changes caused by aberrant H3K9me spreading during heterochromatin misregulation. We found a total of 753 genes under expanded H3K9me3 peaks during stress phase (48 h) that were previously not marked by H3K9me3 in the untreated population (Figure S4C). Surprisingly, of these 753 genes, a subset of only 113 genes were significantly downregulated (Figure 3F). This subset of genes notably included a collection of 21 essential genes, including the mitochondrial LYR (leucine-tyrosine-arginine motif) protein *cup1*+.[21,57] These essential genes are repressed up until the end of stress phase (48 h) after which *clr4*+ silencing and growth rate recovery coincides with their de-repression (Figure 3G). This observation suggests that the downregulation of *cup1*+ and other essential genes proximal to expanding H3K9me3 islands may correlate with poor cell growth during early heterochromatin misregulation. By contrast, during the adapted phase, the only genes both marked by novel H3K9me3 and significantly downregulated were those proximal to the *clr4*+ locus (Figures S4D–S4F). Together, these results indicate that heterochromatin misregulation drives targeted expansion of existing H3K9me domains, leading to aberrant silencing of neighboring essential genes. Additionally, development

(B) H3K9me3 ChIP-seq enrichment centered on *ncRNA.394*. Genomic tracks below show coding transcripts in black, non-coding transcripts in red.
(C) H3K9me3 ChIP-seq enrichment centered on *mei4*+.
(D) H3K9me3 ChIP-seq enrichment centered on *clr4*+.
(E) K-means clustered heatmap (k = 4, 24 kb windows) of H3K9me3 islands during Epe1 depletion at 0, 48, and 120 h in *mst2Δepe1*^{deg}.
(F) Venn diagram depicting downregulated genes by 48 h after Epe1 depletion and genes marked by H3K9me3 selectively at 48 h.
(G) Heatmap depicting downregulated essential genes selectively marked by H3K9me3 at 48 h. Changes in expression are $\log_2$ fold change relative to untreated *mst2Δ epe1*^{deg} cells.

of facultative heterochromatin over the *clr4*+ locus occurs *de novo* and represents rare ectopic nucleation of H3K9me.

Activation of the cellular stress response pathway is required for survival but not adaptive choice

To identify gene pathways relevant to the stress phase of heterochromatin misregulation, we analyzed the set of differentially expressed genes within the stress phase of *mst2Δepe1*^{deg} cells, predicting that it is most likely to contain the most critical population-level transcriptomic features required for adaptation. Enriched GO terms in this set included genes involved in ribosome biogenesis, translation, caffeine and rapamycin treatment, nitrogen depletion, and the core environmental stress response (CESR) (Figures 4A and S5A).[58,59] These results indicate that distinct environmental stress responses overlap significantly with the cellular response to heterochromatin misregulation. Mapping time-dependent changes across these GO categories reveals that the differential expression of cell proliferation and stress response genes subsides following adaptive Clr4 silencing (Figures 4B and S5B–S5F). Considering this apparent relationship, we wanted to interrogate the role that the stress response pathway plays in cell survival during heterochromatin misregulation and adaptive Clr4 silencing.

To interrogate the functional role of CESR during heterochromatin misregulation, we deleted the mitogen-activated protein (MAP) kinase Sty1 in an *mst2Δepe1*^{deg} background. Sty1 regulates the stress response pathway in *S. pombe* by phosphorylating transcription factors that activate the expression of stress response genes, including a majority of CESR genes (Figure 4C).[58] In our original *mst2Δepe1*^{deg} plate assay, when equal numbers of cells were plated, colony numbers were approximately equivalent regardless of Epe1 expression, indicating a high survival rate (Figure 4D). To test how stress response plays into this survival, we similarly plated *mst2Δepe1*^{deg}*sty1Δ*. *mst2Δepe1*^{deg}*sty1Δ* colonies were on average smaller than *mst2Δepe1*^{deg} cells, both pre- and post-Epe1 depletion (Figure 4E). We observed only half as many colonies formed upon plating *mst2Δepe1*^{deg}*sty1Δ* cells upon Epe1 depletion compared with *mst2Δepe1*^{deg} cells (Figure 4F). However, despite lower rates of survival, Epe1-depleted *mst2Δepe1*^{deg}*sty1Δ* colonies showed equally strong adaptive silencing of Clr4 transcription compared with *mst2Δepe1*^{deg} (Figure 4G). This suggests that the activation of stress response pathways is an on-pathway intermediate prior to adaptation but not responsible for driving redistribution of H3K9me.[60] Altogether, these results support Sty1 activity as primarily beneficial for survival during heterochromatin misregulation.

Loss of the RNA-binding protein Red1 attenuates stress and delays adaptive *clr4*+ silencing

We hypothesized that cells must leverage existing heterochromatin nucleation pathways to establish adaptive heterochromatin. Since ChIP-seq identified heterochromatin islands at meiotic genes and ncRNA, we focused on two major heterochromatin nucleation pathways—RNAi (Ago1, Dcr1) and MTREC (Mtl1-Red1 core).[46,56,61,62] Surprisingly, we observed a lesser degree of *clr4*+ silencing in the adapted phase in *red1Δ* cells but not *ago1Δ* or *dcr1Δ* (Figures 5A and S6A).[47] To determine if changes in *clr4*+ silencing correlate with any change in stress and adaptation, we plated cells on solid induction media and also tracked growth rates under continuous culture conditions using eVOLVER (Figures 5B, S6B, and S6C). These approaches confirmed a fitness increase during the stress phase compared with *red1*+ cells, further confirming a distinctive role for Red1 during the stress and subsequent adaptive growth phases. To further quantify and compare loss of fitness during the stress phase, we calculated the mean minimum decrease in growth rates for each eVOLVER experiment (STAR Methods). *red1Δ* cultures displayed a significantly smaller decrease in growth rate, like *mst2Δepe1*^{deg}*clr4Δ*, compared with *mst2Δepe1*^{deg} or RNAi deletions (Figure 5B). We also compared Clr4 mRNA between untreated *red1Δ* and *red1*+ and identified that this lesser degree of *clr4*+ silencing was not due to pre-adaptation in untreated *red1Δ* cells (Figure S6D). Hence, these results suggest that MTREC-mediated Clr4 recruitment may nucleate aberrant heterochromatin during the stress phase to drive downstream adaptation.[63–65]

To determine how H3K9me changes in *mst2Δepe1*^{deg} *red1Δ* cells lead to reduced stress and delayed *clr4*+ silencing, we acquired batch cultures over a 120-h period. ChIP-seq revealed the expansion of H3K9me3 over the *clr4*+ locus appeared restricted relative to *mst2Δepe1*^{deg}*red1*+ cells (Figures 5C and S6E). Additionally, during the stress period, *mst2Δepe1*^{deg}*red1Δ* cells lost several H3K9me3 islands at meiotic genes, consistent with a role for Red1 in nucleating these islands in cycling cells (Figure 5D).[56] Furthermore, these remaining islands in *red1Δ* have less H3K9me3 enrichment at 48 h compared with *red1*+. These H3K9me3 peaks also show slower decay by 120 h, possibly due to weaker *clr4*+ silencing. These observations led us to test if any specific Red1-dependent H3K9me island expansions were primary drivers of the stress phase. For this, we noted an expansion of H3K9me3 from the *mei4*+ locus to a proximal gene, *cdk9*+. Cdk9 is an essential kinase that regulates various aspects of RNA polymerase II transcription including initiation, elongation, and termination.[66–68] Specifically, *cdk9*+ is silenced during the stress phase (24–48 h) but is derepressed once adaptation is complete (120 h) (Figures 3E and 3G). To compensate for Red1 mediated *cdk9*+ silencing, we inserted a second copy of *cdk9*+ at the *leu1*+ locus in *mst2Δepe1*^{deg} ("*2x cdk9*+") (Figure 5E). Our rationale was that the second copy of *cdk9*+ would not be subject to transient silencing in a Red1-dependent manner during the stress phase. Indeed, we observed a weaker growth defect in colony size upon depletion of Epe1, compared with the original strain with one copy of *cdk9*+ (Figure S6F). This was complemented by reduced *clr4*+ silencing similar to *mst2Δepe1*^{deg}*red1Δ*. These observations suggest that aberrant *cdk9*+ silencing is a critical downstream event that promotes stress and subsequent adaptation (Figure 5F). Taken together, these results show which critical heterochromatin island expansions promote epigenetic adaptation.

Adaptive heterochromatin exhibits memory upon re-induction of stress

The *epe1*^{deg} allele enables us to rapidly and reversibly cycle between Epe1 depletion and expression. To test whether cells that had adapted to Epe1 loss also exhibited memory, we restored Epe1 expression in adapted cells for different recovery periods. We refer to these recovery periods as short (24 h), medium (48 h),

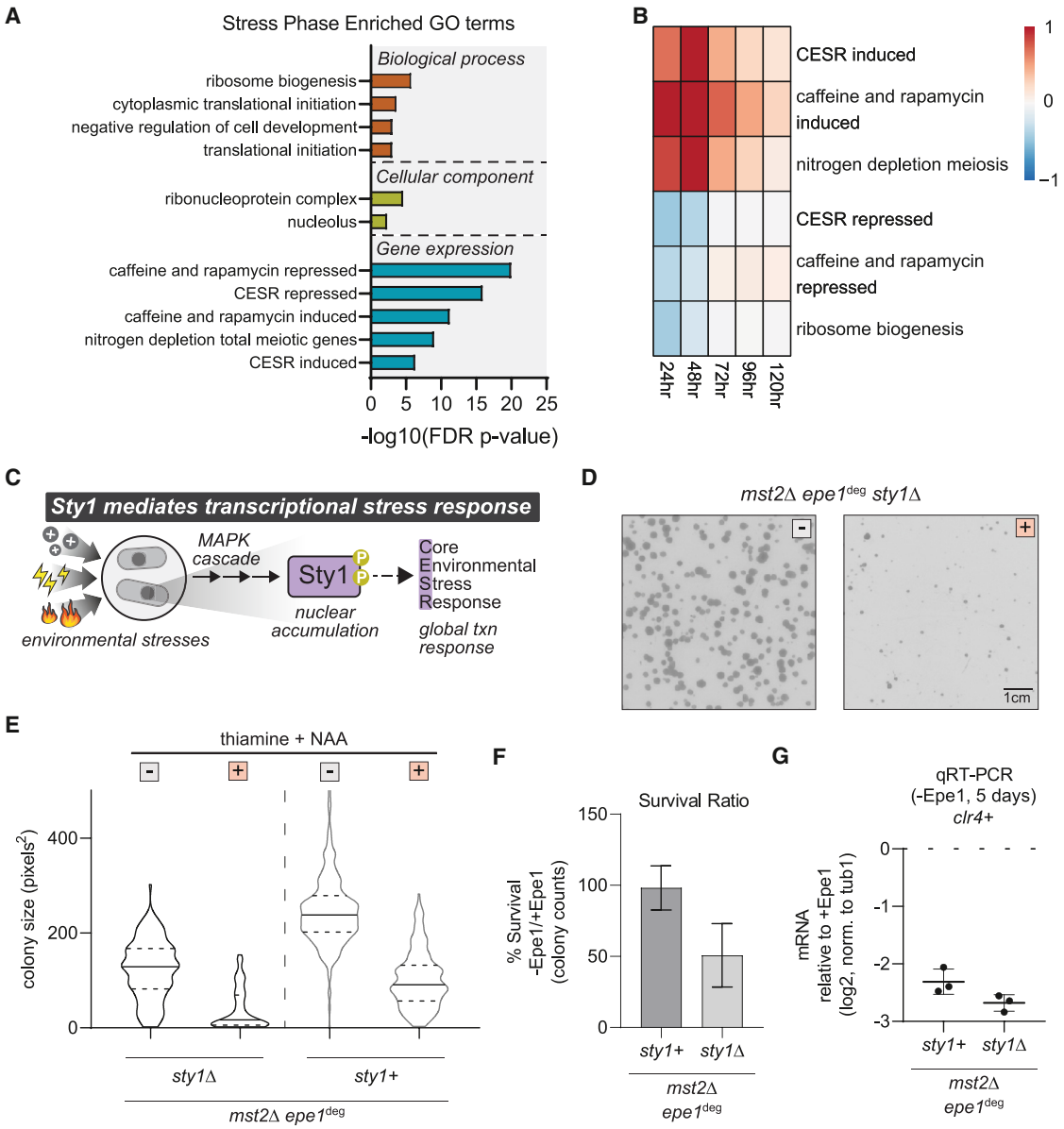

Figure 4. Activation of the cellular stress response pathway is required for survival but not adaptive choice

(A) Selected GO terms for genes differentially expressed within stress phase (48 h of Epe1 depletion).

(B) Heatmap showing average fold change for differentially expressed genes in selected GO categories, relative to untreated *mst2Δepe1*^{deg} cells.

(C) Environmental stresses trigger a stress-activated MAPK cascade that phosphorylates Sty1, which drives a global transcriptional response that includes the core environmental stress response.

(D) Examples of *mst2Δepe1*^{deg}*sty1Δ S. pombe* colonies on solid media after 3 days of growth.

(E) Colony size distribution, in pixel area, under different growth conditions, and quantified after 5 days of growth. Mean and standard deviation of distributions in pixels^2: *mst2Δepe1*^{deg}*sty1Δ* no treatment (123.0 ± 61.9), treated (39.1 ± 43.2); *mst2Δepe1*^{deg} no treatment (246.2 ± 74.6), treated (109.4 ± 64.0).

(F) Percentage of cells that survive following Epe1 depletion for 5 days. Error bars represent standard deviation, $n = 3$.

(G) RT-qPCR measuring *clr4+* RNA levels following 5 days of Epe1 depletion, relative to +Epe1. Error bars represent standard deviation, $n = 3$.

Depletion is pictorially indicated with either a white box for no treatment or an orange box for treatment.

and long (72 h). Following the recovery period, we re-initiated Epe1 depletion to generate a second stress phase (Figures 6A and 6B). If Clr4 silencing is faster during the second stress phase, this would imply that cells have the potential for adaptive memory, where the original adaptation can be recalled more quickly compared to initial adaptive response.

As controls, untreated *mst2Δepe1*^{deg} cells exhibited smaller-sized colonies with substantial heterogeneity upon Epe1 depletion, and adapted cells formed uniformly sized colonies upon sustained Epe1 depletion (Figure 6C). Interestingly, adapted cells that had experienced short 24 h re-expression of Epe1 produced a bimodal distribution of small and large colonies. This

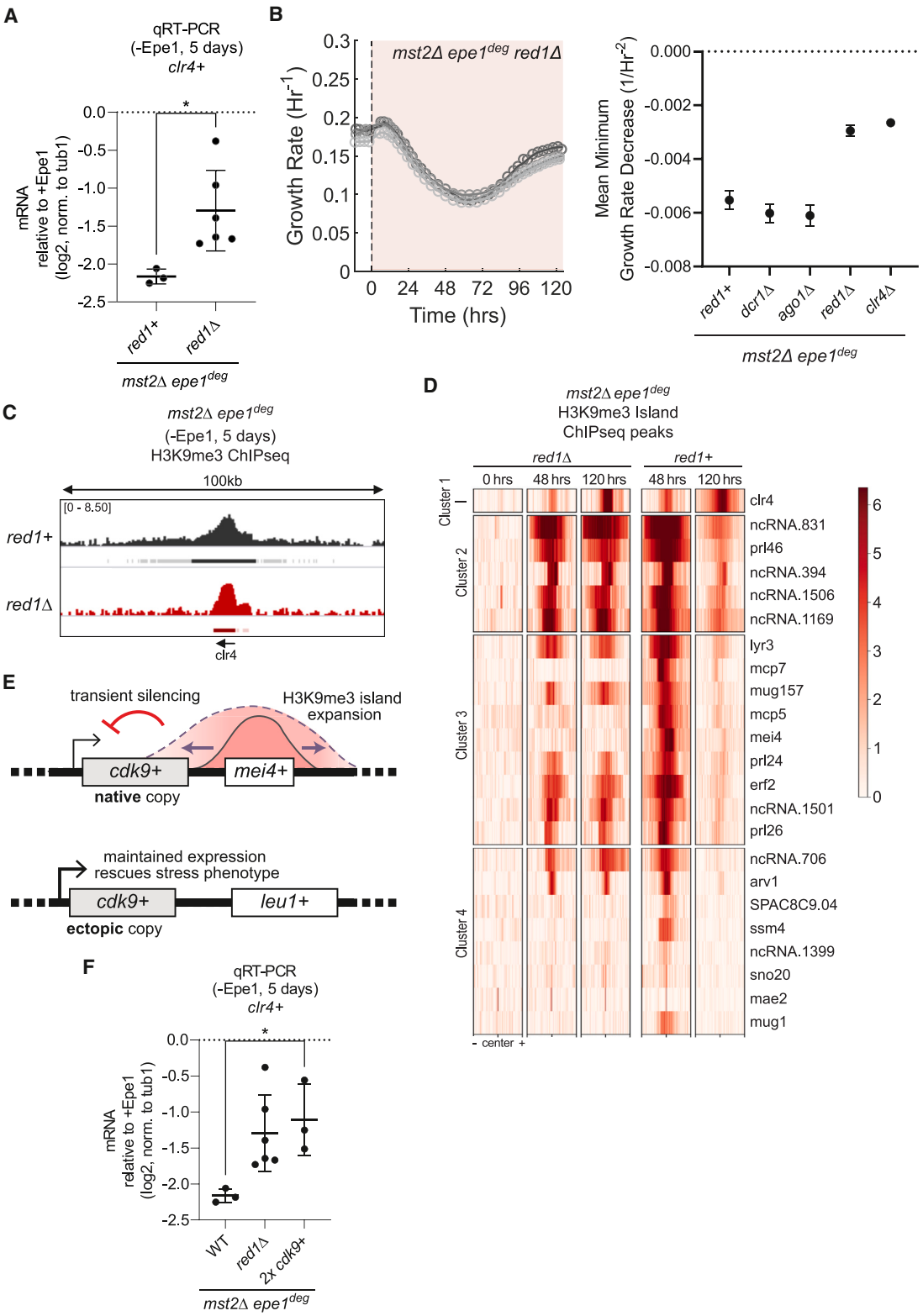

(legend on next page)

suggests that a proportion of short recovery cells had reverted to the untreated state, while others preserved the adapted state during the 2nd stress phase. Medium and long recovery cell populations produced colony size phenotypes that matched untreated cells, suggesting that a prolonged recovery phase (>24 h) led to the complete loss of adaptive memory. Hence, our results reveal that a memory associated with heterochromatin misregulation can persist for about 24 h (~6–8 cell generations) following the removal of the initiating stress.

To measure memory at the chromatin level, we performed H3K9me2 and H3K9me3 ChIP-seq on recovering *mst2Δepe1*^{deg} cells. Short recovery led to a reduction of H3K9me2 and H3K9me3, and by medium recovery, adaptive heterochromatin had decayed to undetectable levels (Figures 6D and S7A). To test if cells in short recovery could re-establish silencing at the *clr4+* locus, we reintroduced heterochromatin stress to short recovery cells by depleting Epe1 a second time. After stress reintroduction, short recovery cells re-established H3K9me3 within 24 h, compared with 72 h in untreated cells (Figure 6D). These changes in Clr4 adaptive heterochromatin are mirrored in *clr4+* transcription; recovering cells expressed *clr4+* at unstressed levels, while cells that have had a prior experience of stress quickly re-established *clr4+* adaptive silencing (Figure 6E). These results show that novel adaptive H3K9me is maintained for several cell divisions during stress recovery, and this residual methylation can encode epigenetic memory to more rapidly re-establish adaptive silencing.

The timescale of adaptive memory can be tuned by histone acetylation

To identify other chromatin-based mechanisms that could tune or enhance adaptive memory duration, we considered the interdependence of H3K9me with other histone modifications. Histone hyperacetylation (H3K9Ac, H3K14Ac, H3K18Ac) and histone turnover are characteristic features of actively transcribed genes, and loss of histone acetylation can promote heterochromatin inheritance.[69,70] Although Mst2 has been deleted in our strains (*mst2Δepe1*^{deg}), it is possible that other histone acetyltransferases could have additive roles in tuning the duration of adaptive memory.[71] We deleted a second acetyltransferase, Gcn5, in a *mst2Δepe1*^{deg} background (*mst2Δgcn5Δepe1*^{deg}). Cells with the *mst2Δgcn5Δepe1*^{deg} genotype grew comparably to *mst2Δepe1*^{deg} prior to Epe1 depletion and had a slightly stronger stress phenotype after loss of Epe1 (Figure S7B). Furthermore, during Epe1 reintroduction and re-depletion, *mst2Δgcn5Δepe1*^{deg} retained large colony sizes even during the long recovery period, implying that these cells may exhibit prolonged, adaptive memory compared with *mst2Δgcn5+* cells (Figure 7A).

Next, we measured other molecular correlates of memory-*clr4+* mRNA levels and H3K9me3 levels at the *clr4+* locus. During each recovery phase, *clr4+* mRNA levels reverted to high levels of transcription, matching what we typically observed in untreated cells. Supporting our model that H3K9me3 is required for epigenetic adaptive memory, all recovering *mst2Δgcn5Δepe1*^{deg} cells retained H3K9me2/3 at the *clr4+* locus, correlating with loss of H3K14Ac (Figures 7B, S7C, and S7D). These results suggest that enhanced H3K9me, arising from the absence of H3K14Ac, can tune the length of adaptive memory. This interdependence on post-translational modifications may allow for cells to rapidly toggle adaptive silencing states, enabling them to extend (or erase) memory of past stress events.

Importantly, although H3K9me3 levels are higher in *gcn5Δ* than in *gcn5+* cells, the modification itself was not sufficient to repress *clr4+* during the recovery phase. Instead, *clr4+* adaptive silencing was reinstated only after Epe1 depletion. When recovering *mst2Δgcn5Δepe1*^{deg} was re-exposed to a 2nd stress, cells re-established Clr4 silencing even though adaptive H3K9me3 maintained a similar distribution compared with the recovering population (Figures 7B and 7C). Our results imply that, while H3K9me has an important role in preserving memory associated with Clr4 silencing, it may not be the only factor that contributes to the silencing process (Figures 6D, 6E, and S7A–S7C). Therefore, we tested whether short recovery cells exhibited unique transcriptional changes that could account for adaptive memory and silencing by performing RNA-seq analysis on short and medium recovery *mst2Δepe1*^{deg} cell populations. Indeed, PCA reveals recovering cells mostly converge to the untreated transcriptome, with some differential expression that is still preserved in short recovery samples (Figure S7E). Importantly, when Epe1 is re-expressed during short recovery, the transcriptional state does not instantaneously revert to the initial untreated state and exhibits differential expression enriched in stress response and metabolic processes (Figure S7F). Since we have previously implicated MTREC in adaptive Clr4 silencing, we examined known Red1 targets.[72,73] We observed significant transcriptional changes in ncRNAs and Red1 targets during the 2nd stress phase, reinforcing the causal role that MTREC has in adaptive silencing (Figures S7G and S7H).

DISCUSSION

Cells can leverage epigenetic pathways to modulate gene expression states in response to environmental change. In fission yeast, H3K9me exhibits adaptive potential when cells encounter various environmental stressors, including anti-fungals, caffeine, or nutrient restriction.[21,39,57,74,75] These stressors

Figure 5. Loss of the RNA-binding protein Red1 attenuates stress and delays adaptive clr4+ silencing

(A) RT-qPCR measuring *clr4+* RNA levels following 5 days of Epe1 depletion, relative to +Epe1. $n = 3,6$. Asterisk indicates $p < 0.05$.

(B) (Left) Real-time monitoring of population growth rates of *mst2Δepe1*^{deg}*red1Δ* eVOLVER cultures. Lines represent moving averages. Orange shaded portion represents Epe1 depletion. (Right) Plot showing mean minimum decrease in growth rate for eVOLVER experiments of the indicated genotypes. $n = 3$.

(C) H3K9me3 ChIP-seq tracks centered on *clr4+* after 5 days of Epe1 depletion in indicated genotypes. Identified peaks denoted in red, enrichment is IP normalized to input (log_2).

(D) Heatmap showing clustered H3K9me3 islands (k = 4 from Figure 3E, 24 kb window), in *mst2Δepe1*^{deg}*red1Δ*.

(E) Schematic for adding an ectopic copy of *cdk9+* at the *leu1+* locus to bypass heterochromatin spreading from *mei4+*.

(F) RT-qPCR measuring *clr4+* RNA levels following 5 days of Epe1 depletion, relative to +Epe1. $n = 3,6$. Asterisk indicates $p < 0.05$.

Error bars represent standard deviation.

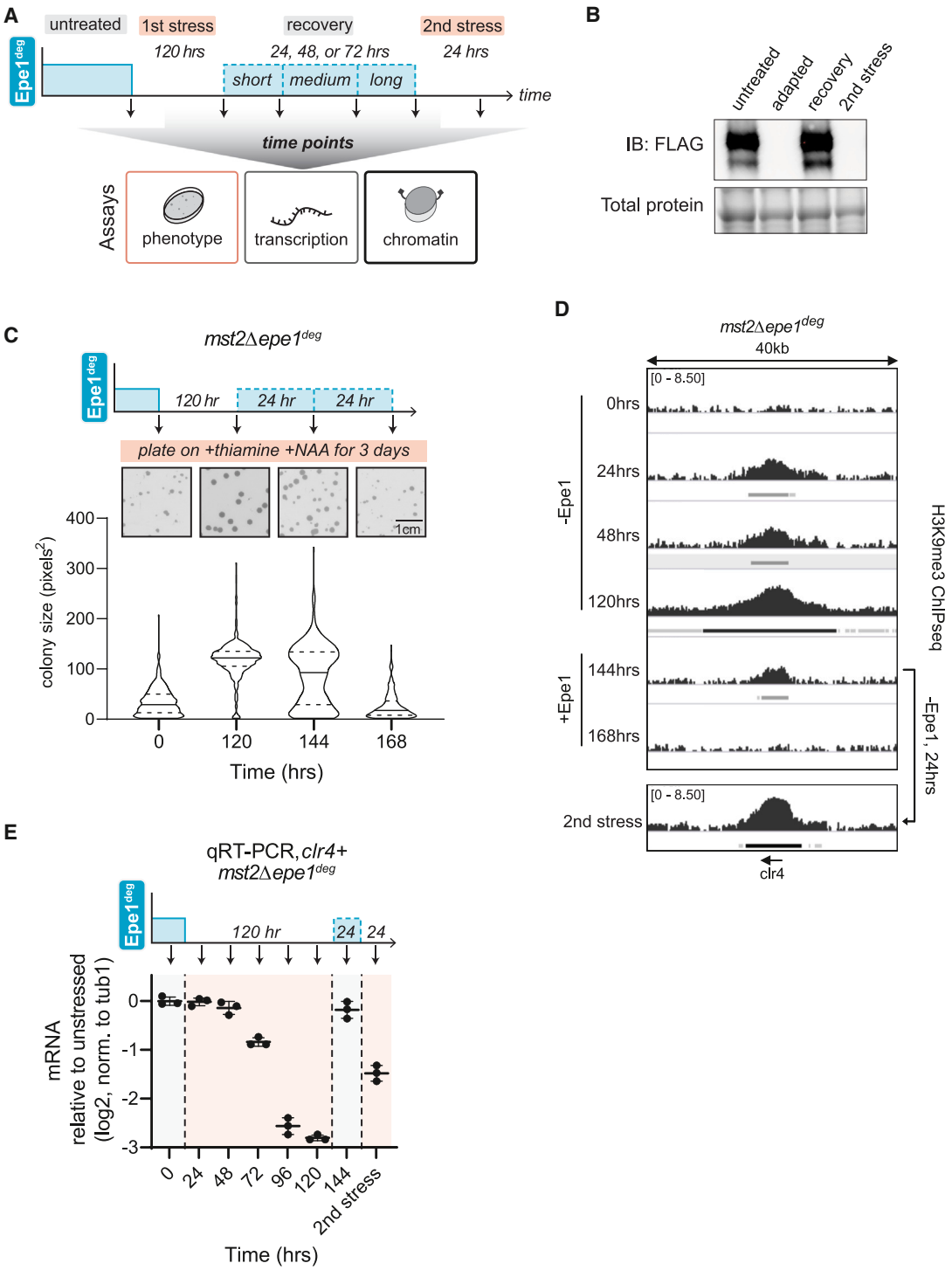

Figure 6. Adaptive heterochromatin exhibits memory upon re-induction of stress

(A) Schematic indicating cycling of Epe1 availability in *mst2Δepe1*^{deg} to measure epigenetic memory at the phenotype, transcription, and chromatin level.

(B) Western blot for Epe1-3xFLAG-AID in *mst2Δepe1*^{deg} cells. Adapted and re-induced adapted cells were treated for Epe1 depletion for a minimum of 24 h.

(C) (Bottom) Colony size distribution of *mst2Δepe1*^{deg} cells after 3 days of growth with Epe1 depletion. (Top) Epe1 expression and snapshots of culture plates. Mean and standard deviation of distributions in pixels^2: 0 h (34.5 ± 27.3), 120 h (118.9 ± 37.6), 144 h (87.3 ± 59.4), 168 h (26.3 ± 25.9).

(D) H3K9me3 ChIP-seq tracks centered on clr4+ after 5 days of Epe1 depletion. Identified peaks denoted in grayscale, and enrichment is IP normalized to input (log_2).

(E) RT-qPCR measuring clr4+ RNA levels following 5 days of Epe1 depletion, relative to +Epe1. Error bars represent standard deviation, $n = 3$.

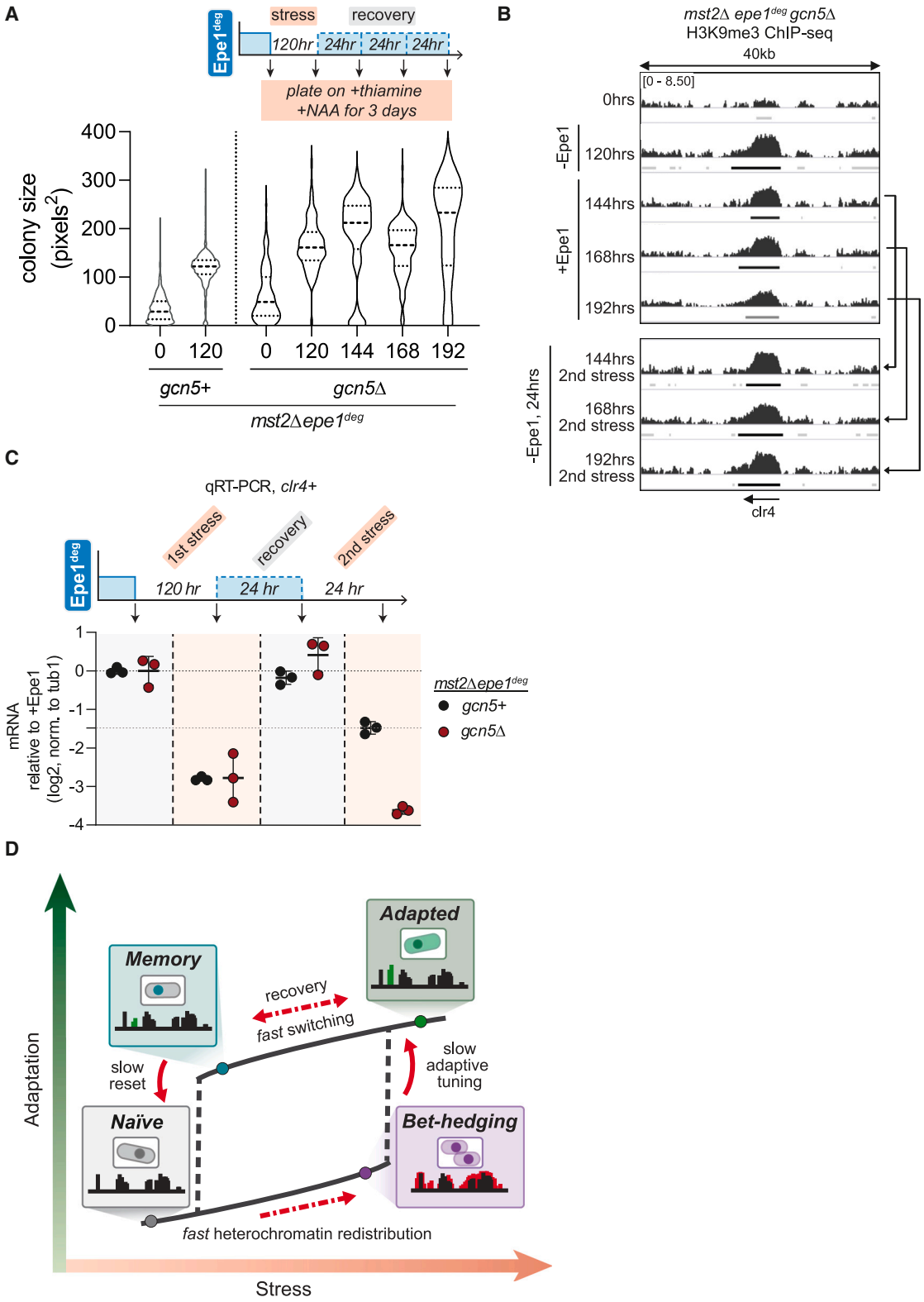

Figure 7. The timescale of adaptive memory can tuned by histone acetylation

(A) Colony size distribution of *mst2Δepe1*^{deg}*gcn5Δ* cells after 3 days of growth with Epe1 depletion. Mean and standard deviation of distributions in pixels^2: 0 h (61.9 ± 53.8), 120 h (166.1 ± 50.9), 144 h (185.8 ± 87.9), 168 h (158.2 ± 54.0), 192 h (201.1 ± 102.3).

(legend continued on next page)

impact two major H3K9me regulators, Epe1 and Mst2, at RNA and protein levels. Our ability to rapidly and reversibly control Epe1 and Mst2 levels enables us to mimic the natural stress response of fission yeast cells, independent of environmental factors. We propose the following model for epigenetic adaptation. Exposure to stress causes Epe1 to undergo proteosome-mediated degradation while Mst2 produces a MYST-domain-deficient isoform.[21,57] This manifests a slow-growth phenotype that allows for an adaptive silencing pathway to redistribute H3K9me. While our inducible depletion system has several controlled variables that separate it from a natural system, it undeniably provides a window into the earliest transcriptomic changes that cells undergo prior to adaptation.

Our system enables the capture of early and intermediate transcriptional states that lead to adaptive silencing of *clr4*+, which would be impossible to visualize using conventional genetic methods.[47] We found that adaptive *clr4*+ silencing takes up to 120 h, which is two orders of magnitude slower than the timescale of Epe1 depletion (~30 min). We propose these dynamics may represent a bet-hedging strategy, where cells reversibly sample transcriptional states that enhance fitness before converging on an optimal solution.[76] Our findings parallel stochastic tuning models in budding yeast, which posit that transcriptional noise is positively selected to promote cell survival in novel environmental conditions.[24,25]

We observed transient activation of genes associated with the CESR, which serve as an on-pathway intermediate preceding adaptation.[60] These dynamics strikingly resemble how cancer cells develop resistance, resulting in poor prognosis and treatment outcomes. For example, glioblastoma cells transiently exit the cell cycle, exhibit slow growth, misregulate H3K27 methylation-dependent epigenetic pathways, and ultimately adapt by entering a state that is refractory to chemotherapeutic interventions.[19] Bacteria also enter slow-growing persister states through the activation of a stress-induced SOS pathway, leading to genetic changes and antibiotic resistance.[8,77] In both instances, slow growth is a common denominator that is triggered by the activation of the stress response pathway. Thus, the activation of stress response pathways may represent a general principle that cells leverage to explore adaptive phenotypes when exposed to novel environments.[60]

It is possible that the unregulated expansion of H3K9me during early heterochromatin misregulation leads to the silencing of essential genes that disrupts fitness and cell survival. This could represent a temporary switch from rapid growth to a slow proliferation state until beneficial adaptations can be acquired. The expansion of heterochromatin domains over essential genes could also act as a filter for stress and adaptive responses. Since the spatial expansion of heterochromatin must build over time, cells would need to experience sustained exposure to a stressor before committing to adaptive H3K9me redistribution, preventing premature adaptive responses to transient environmental perturbations.

Establishing adaptive heterochromatin at the *clr4*+ locus follows unique dynamics that are distinct from H3K9me-spreading at other regions during heterochromatin misregulation. These dynamics suggest active recruitment of heterochromatin initiation and maintenance factors that have adaptive potential, which partially depends on the MTREC subunit, Red1. This raises the possibility that adaptive silencing is mediated by co-transcriptional or post-transcriptional processes that involve non-coding RNA recognition.[56,61,62,78] The expansion of Red1-dependent H3K9me islands during the initial stress phase contributes to activating stress response pathways, thus explaining why deleting Red1 alleviates stress and leads to slower *clr4*+ silencing. How this RNA elimination machinery affects the formation of *de novo* adaptive heterochromatin in other stress contexts, and the extent to which it can be repurposed when cells encounter novel environments, requires further investigation. Our results from relocating *cdk9*+ also support this model and reveal how the arrangement of genes on chromosomes could confer unforeseen advantages during adaptation. This is particularly intriguing given that the *mei4*+ and *cdk9*+ preserve synteny even in the highly diverged *Schizosaccharomyces japonicus*, suggesting how the potential for organisms to adapt could be an emergent property that shapes genome organization.[79] Additionally, our results mirror recent work where inhibition of the human CDK9 ortholog produces transcriptional reprogramming, supporting a model where the inhibition or transient repression of essential genes encourages epigenetic adaptations.[80]

Our unique ability to toggle Epe1 expression enabled us to identify how cells retain adaptive epigenetic memory. This memory is dependent on residual H3K9me that qualitatively resembles earlier work, where adding back Epe1 permanently poises cells in a novel, fixed epigenetic state.[81] By contrast, re-expressing Epe1 in our inducible system leads to total *clr4*+ de-repression, despite significant H3K9me3 being present during recovery. This suggests that H3K9me3 is required for memory, but silencing requires other factors involved in different tiers of transcriptional, co-transcriptional, and post-transcriptional regulation.[82–85] Additionally, Epe1-expressing short recovery cells exhibit unique gene expression signatures, supporting our speculation that memory and adaptive silencing may depend on these novel network-level gene expression changes.[27,54,86] We propose that these features encode a form of cellular hysteresis (Figure 7E).[87] It remains to be seen whether other epigenetic regulators also exhibit hysteresis given the slow kinetics of establishing novel epigenetic states *de novo*.[88]

In conclusion, our inducible system uniquely allowed us to capture highly dynamic changes in gene expression and

(B) H3K9me3 ChIP-seq tracks centered on *clr4*+ after 5 days of Epe1 depletion. Identified peaks denoted in grayscale, and enrichment is IP normalized to input (log_2).

(C) RT-qPCR measuring clr4+ RNA levels following 5 days of Epe1 depletion, relative to +Epe1. Error bars represent standard deviation, $n = 3$.

(D) Heterochromatin-defining H3K9 methylation (H3K9me) can be redistributed across the genome to establish new and potentially adaptive phenotypes. Establishing adaptive H3K9me patterns slowly builds relative to the initiating stress and may serve as a bet-hedging strategy for cells to decipher optimal survival solutions. Upon removal of stress, cells relax to new states rather than revert to the initial ground state. This establishes a tunable memory for future adaptive responses. Cells exhibit history dependence, wherein a prior exposure to stress locks cells in a new transcriptional state that encodes adaptive memory.

chromatin states following acute heterochromatin misregulation, changes that would be otherwise obscured in conventional genetic assays. Using this approach, we reconstructed pathways that cells undertake through adaptation and investigated how the adapted state is preserved across multiple generations. Our findings reveal several distinguishing features of adaptation through epigenetic mechanisms and illuminate strategies by which cells stabilize new gene expression programs to endure acute changes in their environment. Ultimately, we demonstrate a powerful experimental framework to probe adaptation mediated by chromatin regulation, which represents an exciting frontier offering insights into phenotypic plasticity.

Limitations of the study

Our work utilizes an inducible, on-demand system to initiate and track an adaptive epigenetic response upon removing or adding back key heterochromatin regulators in *S. pombe*. Natural stressors would likely elicit additional interspersed transcriptomic changes beyond what we observed. For example, caffeine affects DNA replication, so cells would experience both an adaptive response and replication stress. Nevertheless, understanding how entangled transcriptomic changes enable successful adaptation to stress will be an important area for future investigation. We also noted that *cdk9+* downregulation is part of the initial stress phase leading up to adaptation. Given its widespread roles in transcription, future studies should explore whether downregulating *cdk9+* in response to stress could serve as an initiation signal to trigger epigenetic adaptation. Although we have used Epe1 depletion to trigger heterochromatin misregulation, our studies raise the possibility that other ways of inducing H3K9me deposition at ectopic sites could also contribute to adaptation. One possibility is that non-coding RNA transcription leads to MTREC recruitment causing ectopic H3K9me deposition. This pathway could allow cells to sample the epigenome prior to adaptation. Our current population-level studies do not capture cell-to-cell heterogeneity in the specific choice of *clr4+* as the primary locus enabling the observed epigenetic adaptation. By profiling transcriptomic changes at the single-cell level over time, future work could delineate the diversity of molecular paths individual cells take before converging on an apparent optimal solution.

STAR★METHODS

Detailed methods are provided in the online version of this paper and include the following:

- KEY RESOURCES TABLE
- RESOURCE AVAILABILITY
  - Lead contact
  - Materials availability
  - Data and code availability
- EXPERIMENTAL MODEL AND STUDY PARTICIPANT DETAILS
- METHOD DETAILS
  - Cell culturing and growth quantification
  - Western blotting
  - eVOLVER growth assay
  - qRT-PCR and RNA sequencing analysis
  - Chromatin immunoprecipitation, ChIP-seq library preparation and analysis
- QUANTIFICATION AND STATISTICAL ANALYSIS

SUPPLEMENTAL INFORMATION

Supplemental information can be found online at https://doi.org/10.1016/j.devcel.2024.07.006.

ACKNOWLEDGMENTS

We thank Danesh Moazed for sharing fission yeast strains used in this study. We thank Nidhi Khurana and Gulzhan Raiymbek for their support in obtaining preliminary data during the initial phase of this study. We thank Basila Moochickal Assainar, Amanda Ames, and Sumanth Maheshwaram for their supportive and insightful feedback regarding this study. We thank Tommy V. Vo for helping with ChIP-seq analysis. This work was supported by the National Science Foundation (NSF) (grant no. EF-1921677 to K.R. and A.S.K.), the National Institutes of Health (NIH) (grant nos. R35GM137832 to K.R.; R01EB029483, R01EB027793, and R01AI171100 to A.S.K.), the American Cancer Society (grant no. RSG2211701DMC to K.R.; T32GM007544 to A.L.; and T32GM007315 to M.S.), the Department of Defense Vannevar Bush Faculty Fellowship (no. N00014-20-1-2825 to A.S.K.), and the Schmidt Science Polymath award (no. G-22-63292 to A.S.K.).

AUTHOR CONTRIBUTIONS

Conceptualization, A. Larkin and K.R.; methodology, A. Larkin, C.K., A.S.K., and K.R.; formal analysis, A. Larkin and C.K.; investigation, A. Larkin, C.K., M.S., A. Levashkevich, J.C., D.M.-E., and S.L.; resources, A. Larkin, C.K., M.S., and A. Levashkevich; data curation, A. Larkin and C.K.; writing – original draft, A. Larkin, C.K., A.S.K., and K.R.; writing – review and editing, A. Larkin, C.K., M.S., A. Levashkevich, A.S.K., and K.R.; visualization, A. Larkin and C.K.; funding acquisition, A. Larkin, M.S., A.S.K., and K.R.; supervision, A. Larkin, A.S.K., and K.R.; project administration, A.S.K. and K.R.

DECLARATION OF INTERESTS

The authors declare no competing interests.

Received: July 21, 2023
Revised: April 4, 2024
Accepted: July 9, 2024
Published: August 1, 2024

REFERENCES

1. Brooks, A.N., Turkarslan, S., Beer, K.D., Lo, F.Y., and Baliga, N.S. (2011). Adaptation of cells to new environments. Wiley Interdiscip. Rev. Syst. Biol. Med. *3*, 544–561. https://doi.org/10.1002/wsbm.136.
2. Gasch, A.P., Spellman, P.T., Kao, C.M., Carmel-Harel, O., Eisen, M.B., Storz, G., Botstein, D., and Brown, P.O. (2000). Genomic Expression Programs in the Response of Yeast Cells to Environmental Changes. Mol. Biol. Cell *11*, 4241–4257. https://doi.org/10.1091/mbc.11.12.4241.
3. B. Alberts, ed. (2002). Molecular Biology of the Cell, Fourth Edition (Garland Science).
4. Fisher, M.C., Alastruey-Izquierdo, A., Berman, J., Bicanic, T., Bignell, E.M., Bowyer, P., Bromley, M., Brüggemann, R., Garber, G., Cornely, O.A., et al. (2022). Tackling the emerging threat of antifungal resistance to human health. Nat. Rev. Microbiol. *20*, 557–571. https://doi.org/10.1038/s41579-022-00720-1.
5. Flavahan, W.A., Gaskell, E., and Bernstein, B.E. (2017). Epigenetic plasticity and the hallmarks of cancer. Science *357*, eaal2380. https://doi.org/10.1126/science.aal2380.
6. Baker, S., Thomson, N., Weill, F.-X., and Holt, K.E. (2018). Genomic insights into the emergence and spread of antimicrobial-resistant bacterial pathogens. Science *360*, 733–738. https://doi.org/10.1126/science.aar3777.
7. Luria, S.E., and Delbrück, M. (1943). MUTATIONS OF BACTERIA FROM VIRUS SENSITIVITY TO VIRUS RESISTANCE. Genetics *28*, 491–511. https://doi.org/10.1093/genetics/28.6.491.

8. McKenzie, G.J., Harris, R.S., Lee, P.L., and Rosenberg, S.M. (2000). The SOS response regulates adaptive mutation. Proc. Natl. Acad. Sci. USA *97*, 6646–6651. https://doi.org/10.1073/pnas.120161797.

9. Ravikumar, A., Arzumanyan, G.A., Obadi, M.K.A., Javanpour, A.A., and Liu, C.C. (2018). Scalable, Continuous Evolution of Genes at Mutation Rates above Genomic Error Thresholds. Cell *175*, 1946–1957.e13. https://doi.org/10.1016/j.cell.2018.10.021.

10. Masel, J., and Trotter, M.V. (2010). Robustness and Evolvability. Trends Genet. *26*, 406–414. https://doi.org/10.1016/j.tig.2010.06.002.

11. Stajic, D., Bank, C., and Gordo, I. (2022). Adaptive Potential of Epigenetic Switching During Adaptation to Fluctuating Environments. Genome Biol. Evol. *14*, evac065. https://doi.org/10.1093/gbe/evac065.

12. Allis, C.D., and Jenuwein, T. (2016). The molecular hallmarks of epigenetic control. Nat. Rev. Genet. *17*, 487–500. https://doi.org/10.1038/nrg.2016.59.

13. Stajic, D., Perfeito, L., and Jansen, L.E.T. (2019). Epigenetic gene silencing alters the mechanisms and rate of evolutionary adaptation. Nat. Ecol. Evol. *3*, 491–498. https://doi.org/10.1038/s41559-018-0781-2.

14. Casadesús, J., and Low, D. (2006). Epigenetic Gene Regulation in the Bacterial World. Microbiol. Mol. Biol. Rev. *70*, 830–856. https://doi.org/10.1128/MMBR.00016-06.

15. Kussell, E., and Leibler, S. (2005). Phenotypic Diversity, Population Growth, and Information in Fluctuating Environments. Science *309*, 2075–2078. https://doi.org/10.1126/science.1114383.

16. Thattai, M., and van Oudenaarden, A. (2004). Stochastic Gene Expression in Fluctuating Environments. Genetics *167*, 523–530. https://doi.org/10.1534/genetics.167.1.523.

17. Calo, S., Shertz-Wall, C., Lee, S.C., Bastidas, R.J., Nicolás, F.E., Granek, J.A., Mieczkowski, P., Torres-Martínez, S., Ruiz-Vázquez, R.M., Cardenas, M.E., and Heitman, J. (2014). Antifungal drug resistance evoked via RNAi-dependent epimutations. Nature *513*, 555–558. https://doi.org/10.1038/nature13575.

18. Guler, G.D., Tindell, C.A., Pitti, R., Wilson, C., Nichols, K., KaiWai Cheung, T., Kim, H.-J., Wongchenko, M., Yan, Y., Haley, B., et al. (2017). Repression of Stress-Induced LINE-1 Expression Protects Cancer Cell Subpopulations from Lethal Drug Exposure. Cancer Cell *32*, 221–237.e13. https://doi.org/10.1016/j.ccell.2017.07.002.

19. Liau, B.B., Sievers, C., Donohue, L.K., Gillespie, S.M., Flavahan, W.A., Miller, T.E., Venteicher, A.S., Hebert, C.H., Carey, C.D., Rodig, S.J., et al. (2017). Adaptive Chromatin Remodeling Drives Glioblastoma Stem Cell Plasticity and Drug Tolerance. Cell Stem Cell *20*, 233–246.e7. https://doi.org/10.1016/j.stem.2016.11.003.

20. Sharma, S.V., Lee, D.Y., Li, B., Quinlan, M.P., Takahashi, F., Maheswaran, S., McDermott, U., Azizian, N., Zou, L., Fischbach, M.A., et al. (2010). A Chromatin-Mediated Reversible Drug-Tolerant State in Cancer Cell Subpopulations. Cell *141*, 69–80. https://doi.org/10.1016/j.cell.2010.02.027.

21. Torres-Garcia, S., Yaseen, I., Shukla, M., Audergon, P.N.C.B., White, S.A., Pidoux, A.L., and Allshire, R.C. (2020). Epigenetic gene silencing by heterochromatin primes fungal resistance. Nature *585*, 453–458. https://doi.org/10.1038/s41586-020-2706-x.

22. Halfmann, R., Jarosz, D.F., Jones, S.K., Chang, A., Lancaster, A.K., and Lindquist, S. (2012). Prions are a common mechanism for phenotypic inheritance in wild yeasts. Nature *482*, 363–368. https://doi.org/10.1038/nature10875.

23. True, H.L., and Lindquist, S.L. (2000). A yeast prion provides a mechanism for genetic variation and phenotypic diversity. Nature *407*, 477–483. https://doi.org/10.1038/35035005.

24. David, L., Stolovicki, E., Haziz, E., and Braun, E. (2010). Inherited adaptation of genome-rewired cells in response to a challenging environment. HFSP J. *4*, 131–141. https://doi.org/10.2976/1.3353782.

25. Freddolino, P.L., Yang, J., Momen-Roknabadi, A., and Tavazoie, S. (2018). Stochastic tuning of gene expression enables cellular adaptation in the absence of pre-existing regulatory circuitry. eLife *7*, e31867. https://doi.org/10.7554/eLife.31867.

26. Kiani, K., Sanford, E.M., Goyal, Y., and Raj, A. (2022). Changes in chromatin accessibility are not concordant with transcriptional changes for single-factor perturbations. Mol. Syst. Biol. *18*, e10979. https://doi.org/10.15252/msb.202210979.

27. Parmentier, R., Racine, L., Moussy, A., Chantalat, S., Sudharshan, R., Papili Gao, N., Stockholm, D., Corre, G., Fourel, G., Deleuze, J.-F., et al. (2022). Global genome decompaction leads to stochastic activation of gene expression as a first step toward fate commitment in human hematopoietic cells. PLoS Biol. *20*, e3001849. https://doi.org/10.1371/journal.pbio.3001849.

28. Shaffer, S.M., Emert, B.L., Reyes Hueros, R.A., Cote, C., Harmange, G., Schaff, D.L., Sizemore, A.E., Gupte, R., Torre, E., Singh, A., et al. (2020). Memory Sequencing Reveals Heritable Single-Cell Gene Expression Programs Associated with Distinct Cellular Behaviors. Cell *182*, 947–959.e17. https://doi.org/10.1016/j.cell.2020.07.003.

29. Shaffer, S.M., Dunagin, M.C., Torborg, S.R., Torre, E.A., Emert, B., Krepler, C., Beqiri, M., Sproesser, K., Brafford, P.A., Xiao, M., et al. (2017). Rare cell variability and drug-induced reprogramming as a mode of cancer drug resistance. Nature *546*, 431–435. https://doi.org/10.1038/nature22794.

30. Tagkopoulos, I., Liu, Y.-C., and Tavazoie, S. (2008). Predictive Behavior Within Microbial Genetic Networks. Science *320*, 1313–1317. https://doi.org/10.1126/science.1154456.

31. Raj, A., and van Oudenaarden, A. (2008). Nature, Nurture, or Chance: Stochastic Gene Expression and Its Consequences. Cell *135*, 216–226. https://doi.org/10.1016/j.cell.2008.09.050.

32. Audergon, P.N.C.B., Catania, S., Kagansky, A., Tong, P., Shukla, M., Pidoux, A.L., and Allshire, R.C. (2015). Epigenetics. Restricted epigenetic inheritance of H3K9 methylation. Science *348*, 132–135. https://doi.org/10.1126/science.1260638.

33. Light, W.H., Brickner, D.G., Brand, V.R., and Brickner, J.H. (2010). Interaction of a DNA Zip Code with the Nuclear Pore Complex Promotes H2A.Z Incorporation and INO1 Transcriptional Memory. Mol. Cell *40*, 112–125. https://doi.org/10.1016/j.molcel.2010.09.007.

34. Park, M., Patel, N., Keung, A.J., and Khalil, A.S. (2019). Engineering Epigenetic Regulation Using Synthetic Read-Write Modules. Cell *176*, 227–238.e20. https://doi.org/10.1016/j.cell.2018.11.002.

35. Ragunathan, K., Jih, G., and Moazed, D. (2015). Epigenetic inheritance uncoupled from sequence-specific recruitment. Science *348*, 1258699. https://doi.org/10.1126/science.1258699.

36. Sump, B., Brickner, D.G., D'Urso, A., Kim, S.H., and Brickner, J.H. (2022). Mitotically heritable, RNA polymerase II-independent H3K4 dimethylation stimulates INO1 transcriptional memory. eLife *11*, e77646. https://doi.org/10.7554/eLife.77646.

37. Allshire, R.C., and Madhani, H.D. (2018). Ten principles of heterochromatin formation and function. Nat. Rev. Mol. Cell Biol. *19*, 229–244. https://doi.org/10.1038/nrm.2017.119.

38. Duempelmann, L., Mohn, F., Shimada, Y., Oberti, D., Andriollo, A., Lochs, S., and Bühler, M. (2019). Inheritance of a Phenotypically Neutral Epimutation Evokes Gene Silencing in Later Generations. Mol. Cell *74*, 534–541.e4. https://doi.org/10.1016/j.molcel.2019.02.009.

39. Gallagher, P.S., Larkin, M., Thillainadesan, G., Dhakshnamoorthy, J., Balachandran, V., Xiao, H., Wellman, C., Chatterjee, R., Wheeler, D., and Grewal, S.I.S. (2018). Iron homeostasis regulates facultative heterochromatin assembly in adaptive genome control. Nat. Struct. Mol. Biol. *25*, 372–383. https://doi.org/10.1038/s41594-018-0056-2.

40. Halic, M., and Moazed, D. (2010). Dicer-Independent Primal RNAs Trigger RNAi and Heterochromatin Formation. Cell *140*, 504–516. https://doi.org/10.1016/j.cell.2010.01.019.

41. Iglesias, N., Currie, M.A., Jih, G., Paulo, J.A., Siuti, N., Kalocsay, M., Gygi, S.P., and Moazed, D. (2018). Automethylation-induced conformational

switch in Clr4 (Suv39h) maintains epigenetic stability. Nature *560*, 504–508. https://doi.org/10.1038/s41586-018-0398-2.

42. Kowalik, K.M., Shimada, Y., Flury, V., Stadler, M.B., Batki, J., and Bühler, M. (2015). The Paf1 complex represses small-RNA-mediated epigenetic gene silencing. Nature *520*, 248–252. https://doi.org/10.1038/nature14337.
43. Parsa, J.-Y., Boudoukha, S., Burke, J., Homer, C., and Madhani, H.D. (2018). Polymerase pausing induced by sequence-specific RNA-binding protein drives heterochromatin assembly. Genes Dev. *32*, 953–964. https://doi.org/10.1101/gad.310136.117.
44. Pisacane, P., and Halic, M. (2017). Tailing and degradation of Argonaute-bound small RNAs protect the genome from uncontrolled RNAi. Nat. Commun. *8*, 15332. https://doi.org/10.1038/ncomms15332.
45. Wei, Y., Lee, N.N., Pan, L., Dhakshnamoorthy, J., Sun, L.-L., Zofall, M., Wheeler, D., and Grewal, S.I.S. (2021). TOR targets an RNA processing network to regulate facultative heterochromatin, developmental gene expression and cell proliferation. Nat. Cell Biol. *23*, 243–256. https://doi.org/10.1038/s41556-021-00631-y.
46. Yamanaka, S., Mehta, S., Reyes-Turcu, F.E., Zhuang, F., Fuchs, R.T., Rong, Y., Robb, G.B., and Grewal, S.I.S. (2013). RNAi triggered by specialized machinery silences developmental genes and retrotransposons. Nature *493*, 557–560. https://doi.org/10.1038/nature11716.
47. Wang, J., Reddy, B.D., and Jia, S. (2015). Rapid epigenetic adaptation to uncontrolled heterochromatin spreading. eLife *4*, e06179. https://doi.org/10.7554/eLife.06179.
48. Basi, G., Schmid, E., and Maundrell, K. (1993). TATA box mutations in the Schizosaccharomyces pombe nmt1 promoter affect transcription efficiency but not the transcription start point or thiamine repressibility. Gene *123*, 131–136. https://doi.org/10.1016/0378-1119(93)90552-E.
49. Kanke, M., Nishimura, K., Kanemaki, M., Kakimoto, T., Takahashi, T.S., Nakagawa, T., and Masukata, H. (2011). Auxin-inducible protein depletion system in fission yeast. BMC Cell Biol. *12*, 8. https://doi.org/10.1186/1471-2121-12-8.
50. Lenski, R.E., Wiser, M.J., Ribeck, N., Blount, Z.D., Nahum, J.R., Morris, J.J., Zaman, L., Turner, C.B., Wade, B.D., Maddamsetti, R., et al. (2015). Sustained fitness gains and variability in fitness trajectories in the long-term evolution experiment with *Escherichia coli*. Proc. Biol. Sci. *282*, 20152292. https://doi.org/10.1098/rspb.2015.2292.
51. Heins, Z.J., Mancuso, C.P., Kiriakov, S., Wong, B.G., Bashor, C.J., and Khalil, A.S. (2019). Designing Automated, High-throughput, Continuous Cell Growth Experiments Using eVOLVER. J. Vis. Exp. *147*, 59652. https://doi.org/10.3791/59652.
52. Wong, B.G., Mancuso, C.P., Kiriakov, S., Bashor, C.J., and Khalil, A.S. (2018). Precise, automated control of conditions for high-throughput growth of yeast and bacteria with eVOLVER. Nat. Biotechnol. *36*, 614–623. https://doi.org/10.1038/nbt.4151.
53. García-Ruano, D., Jain, A., Heins, Z.J., Wong, B.G., Yimer Wolle, E., Khalil, A.S., and Coudreuse, D. (2023). Long-term evolution of proliferating cells using the eVOLVER platform. Open Biol. *13*, 230118. https://doi.org/10.1098/rsob.230118.
54. Huang, S. (2022). Towards a unification of the 2 meanings of "epigenetics.". PLoS Biol. *20*, e3001944. https://doi.org/10.1371/journal.pbio.3001944.
55. Zhong, Z., Wong, B.G., Ravikumar, A., Arzumanyan, G.A., Khalil, A.S., and Liu, C.C. (2020). Automated Continuous Evolution of Proteins *in Vivo*. ACS Synth. Biol. *9*, 1270–1276. https://doi.org/10.1021/acssynbio.0c00135.
56. Zofall, M., Yamanaka, S., Reyes-Turcu, F.E., Zhang, K., Rubin, C., and Grewal, S.I.S. (2012). RNA Elimination Machinery Targeting Meiotic mRNAs Promotes Facultative Heterochromatin Formation. Science *335*, 96–100. https://doi.org/10.1126/science.1211651.
57. Yaseen, I., White, S.A., Torres-Garcia, S., Spanos, C., Lafos, M., Gaberdiel, E., Yeboah, R., El Karoui, M., Rappsilber, J., Pidoux, A.L., and Allshire, R.C. (2022). Proteasome-dependent truncation of the negative heterochromatin regulator Epe1 mediates antifungal resistance. Nat. Struct. Mol. Biol. *29*, 745–758. https://doi.org/10.1038/s41594-022-00801-y.
58. Chen, D., Toone, W.M., Mata, J., Lyne, R., Burns, G., Kivinen, K., Brazma, A., Jones, N., and Bähler, J. (2003). Global Transcriptional Responses of Fission Yeast to Environmental Stress. Mol. Biol. Cell *14*, 214–229. https://doi.org/10.1091/mbc.e02-08-0499.
59. Rubio, A., Ghosh, S., Mülleder, M., Ralser, M., and Mata, J. (2021). Ribosome profiling reveals ribosome stalling on tryptophan codons and ribosome queuing upon oxidative stress in fission yeast. Nucleic Acids Res. *49*, 383–399. https://doi.org/10.1093/nar/gkaa1180.
60. Ho, Y.-H., and Gasch, A.P. (2015). Exploiting the yeast stress-activated signaling network to inform on stress biology and disease signaling. Curr. Genet. *61*, 503–511. https://doi.org/10.1007/s00294-015-0491-0.
61. Egan, E.D., Braun, C.R., Gygi, S.P., and Moazed, D. (2014). Post-transcriptional regulation of meiotic genes by a nuclear RNA silencing complex. RNA *20*, 867–881. https://doi.org/10.1261/rna.044479.114.
62. Lee, N.N., Chalamcharla, V.R., Reyes-Turcu, F., Mehta, S., Zofall, M., Balachandran, V., Dhakshnamoorthy, J., Taneja, N., Yamanaka, S., Zhou, M., and Grewal, S.I. (2013). Mtr4-like Protein Coordinates Nuclear RNA Processing for Heterochromatin Assembly and for Telomere Maintenance. Cell *155*, 1061–1074. https://doi.org/10.1016/j.cell.2013.10.027.
63. Dobrev, N., Ahmed, Y.L., Sivadas, A., Soni, K., Fischer, T., and Sinning, I. (2021). The zinc-finger protein Red1 orchestrates MTREC submodules and binds the Mtl1 helicase arch domain. Nat. Commun. *12*, 3456. https://doi.org/10.1038/s41467-021-23565-3.
64. Foucher, A.-E., Touat-Todeschini, L., Juarez-Martinez, A.B., Rakitch, A., Laroussi, H., Karczewski, C., Acajjaoui, S., Soler-López, M., Cusack, S., Mackereth, C.D., et al. (2022). Structural analysis of Red1 as a conserved scaffold of the RNA-targeting MTREC/PAXT complex. Nat. Commun. *13*, 4969. https://doi.org/10.1038/s41467-022-32542-3.
65. Soni, K., Sivadas, A., Horvath, A., Dobrev, N., Hayashi, R., Kiss, L., Simon, B., Wild, K., Sinning, I., and Fischer, T. (2023). Mechanistic insights into RNA surveillance by the canonical poly(A) polymerase Pla1 of the MTREC complex. Nat. Commun. *14*, 772. https://doi.org/10.1038/s41467-023-36402-6.
66. Pei, Y., Schwer, B., and Shuman, S. (2003). Interactions between Fission Yeast Cdk9, Its Cyclin Partner Pch1, and mRNA Capping Enzyme Pct1 Suggest an Elongation Checkpoint for mRNA Quality Control. J. Biol. Chem. *278*, 7180–7188. https://doi.org/10.1074/jbc.M211713200.
67. Parua, P.K., Booth, G.T., Sansó, M., Benjamin, B., Tanny, J.C., Lis, J.T., and Fisher, R.P. (2018). A Cdk9–PP1 switch regulates the elongation–termination transition of RNA polymerase II. Nature *558*, 460–464. https://doi.org/10.1038/s41586-018-0214-z.
68. Anshabo, A.T., Milne, R., Wang, S., and Albrecht, H. (2021). CDK9: A Comprehensive Review of Its Biology, and Its Role as a Potential Target for Anti-Cancer Agents. Front. Oncol. *11*, 678559. https://doi.org/10.3389/fonc.2021.678559.
69. Aygün, O., Mehta, S., and Grewal, S.I.S. (2013). HDAC-mediated suppression of histone turnover promotes epigenetic stability of heterochromatin. Nat. Struct. Mol. Biol. *20*, 547–554. https://doi.org/10.1038/nsmb.2565.
70. Johnsson, A., Durand-Dubief, M., Xue-Franzén, Y., Rönnerblad, M., Ekwall, K., and Wright, A. (2009). HAT–HDAC interplay modulates global histone H3K14 acetylation in gene-coding regions during stress. EMBO Rep. *10*, 1009–1014. https://doi.org/10.1038/embor.2009.127.
71. Zofall, M., Sandhu, R., Holla, S., Wheeler, D., and Grewal, S.I.S. (2022). Histone deacetylation primes self-propagation of heterochromatin domains to promote epigenetic inheritance. Nat. Struct. Mol. Biol. *29*, 898–909. https://doi.org/10.1038/s41594-022-00830-7.
72. Bitton, D.A., Schubert, F., Dey, S., Okoniewski, M., Smith, G.C., Khadayate, S., Pancaldi, V., Wood, V., and Bähler, J. (2015). AnGeLi: A Tool for the Analysis of Gene Lists from Fission Yeast. Front. Genet. *6*, 330. https://doi.org/10.3389/fgene.2015.00330.

73. Hasan, A., Cotobal, C., Duncan, C.D.S., and Mata, J. (2014). Systematic Analysis of the Role of RNA-Binding Proteins in the Regulation of RNA Stability. PLoS Genet. *10*, e1004684. https://doi.org/10.1371/journal.pgen.1004684.

74. Bao, K., Shan, C.-M., Chen, X., Raiymbek, G., Monroe, J.G., Fang, Y., Toda, T., Koutmou, K.S., Ragunathan, K., Lu, C., et al. (2022). The cAMP signaling pathway regulates Epe1 protein levels and heterochromatin assembly. PLoS Genet. *18*, e1010049. https://doi.org/10.1371/journal.pgen.1010049.

75. Hirai, H., Takemata, N., Tamura, M., and Ohta, K. (2022). Facultative heterochromatin formation in rDNA is essential for cell survival during nutritional starvation. Nucleic Acids Res. *50*, 3727–3744. https://doi.org/10.1093/nar/gkac175.

76. Ogura, M., Wakaiki, M., and Preciado, V.M. (2016). Dynamic analysis of bet-hedging strategies as a protection mechanism against environmental fluctuations. In 2016 IEEE 55th Conference on Decision and Control (CDC) (IEEE), pp. 4178–4183. https://doi.org/10.1109/CDC.2016.7798903.

77. Cairns, J., Overbaugh, J., and Miller, S. (1988). The origin of mutants. Nature *335*, 142–145. https://doi.org/10.1038/335142a0.

78. Khanduja, J.S., Joh, R.I., Perez, M.M., Paulo, J.A., Palmieri, C.M., Zhang, J., Gulka, A.O.D., Haas, W., Gygi, S.P., and Motamedi, M. (2024). RNA quality control factors nucleate Clr4/SUV39H and trigger constitutive heterochromatin assembly. Cell *187*, 3262–3283.e23. https://doi.org/10.1016/j.cell.2024.04.042.

79. Rhind, N., Chen, Z., Yassour, M., Thompson, D.A., Haas, B.J., Habib, N., Wapinski, I., Roy, S., Lin, M.F., Heiman, D.I., et al. (2011). Comparative Functional Genomics of the Fission Yeasts. Science *332*, 930–936. https://doi.org/10.1126/science.1203357.

80. Thieme, E., Bruss, N., Sun, D., Dominguez, E.C., Coleman, D., Liu, T., Roleder, C., Martinez, M., Garcia-Mansfield, K., Ball, B., et al. (2023). CDK9 inhibition induces epigenetic reprogramming revealing strategies to circumvent resistance in lymphoma. Mol. Cancer *22*, 64. https://doi.org/10.1186/s12943-023-01762-6.

81. Sorida, M., Hirauchi, T., Ishizaki, H., Kaito, W., Shimada, A., Mori, C., Chikashige, Y., Hiraoka, Y., Suzuki, Y., Ohkawa, Y., et al. (2019). Regulation of ectopic heterochromatin-mediated epigenetic diversification by the JmjC family protein Epe1. PLoS Genet. *15*, e1008129. https://doi.org/10.1371/journal.pgen.1008129.

82. Marina, D.B., Shankar, S., Natarajan, P., Finn, K.J., and Madhani, H.D. (2013). A conserved ncRNA-binding protein recruits silencing factors to heterochromatin through an RNAi-independent mechanism. Genes Dev. *27*, 1851–1856. https://doi.org/10.1101/gad.226019.113.

83. Thillainadesan, G., Xiao, H., Holla, S., Dhakshnamoorthy, J., Jenkins, L.M.M., Wheeler, D., and Grewal, S.I.S. (2020). Conserved protein Pir2ARS2 mediates gene repression through cryptic introns in lncRNAs. Nat. Commun. *11*, 2412. https://doi.org/10.1038/s41467-020-16280-y.

84. Vo, T.V., Dhakshnamoorthy, J., Larkin, M., Zofall, M., Thillainadesan, G., Balachandran, V., Holla, S., Wheeler, D., and Grewal, S.I.S. (2019). CPF Recruitment to Non-canonical Transcription Termination Sites Triggers Heterochromatin Assembly and Gene Silencing. Cell Rep. *28*, 267–281.e5. https://doi.org/10.1016/j.celrep.2019.05.107.

85. Bühler, M., Spies, N., Bartel, D.P., and Moazed, D. (2008). TRAMP-mediated RNA surveillance prevents spurious entry of RNAs into the Schizosaccharomyces pombe siRNA pathway. Nat. Struct. Mol. Biol. *15*, 1015–1023. https://doi.org/10.1038/nsmb.1481.

86. Holoch, D., Wassef, M., Lövkvist, C., Zielinski, D., Aflaki, S., Lombard, B., Héry, T., Loew, D., Howard, M., and Margueron, R. (2021). A cis-acting mechanism mediates transcriptional memory at Polycomb target genes in mammals. Nat. Genet. *53*, 1686–1697. https://doi.org/10.1038/s41588-021-00964-2.

87. Kramer, B.P., and Fussenegger, M. (2005). Hysteresis in a synthetic mammalian gene network. Proc. Natl. Acad. Sci. USA *102*, 9517–9522. https://doi.org/10.1073/pnas.0500345102.

88. Tatarakis, A., Saini, H., and Moazed, D. (2023). Requirements for establishment and epigenetic stability of mammalian heterochromatin. Preprint at bioRxiv. https://doi.org/10.1101/2023.02.27.530221.

89. Dobin, A., Davis, C.A., Schlesinger, F., Drenkow, J., Zaleski, C., Jha, S., Batut, P., Chaisson, M., and Gingeras, T.R. (2013). STAR: ultrafast universal RNA-seq aligner. Bioinformatics *29*, 15–21. https://doi.org/10.1093/bioinformatics/bts635.

90. Andrews, S. (2010). FastQC: A Quality Control Tool for High Throughput Sequence Data. Available online at: http://www.bioinformatics.babraham.ac.uk/projects/fastqc/.

91. Bolger, A.M., Lohse, M., and Usadel, B. (2014). Trimmomatic: a flexible trimmer for Illumina sequence data. Bioinformatics *30*, 2114–2120. https://doi.org/10.1093/bioinformatics/btu170.

92. Danecek, P., Bonfield, J.K., Liddle, J., Marshall, J., Ohan, V., Pollard, M.O., Whitwham, A., Keane, T., McCarthy, S.A., Davies, R.M., et al. (2021). Twelve years of SAMtools and BCFtools. GigaScience *10*, giab008. https://doi.org/10.1093/gigascience/giab008.

93. Love, M.I., Huber, W., and Anders, S. (2014). Moderated estimation of fold change and dispersion for RNA-seq data with DESeq2. Genome Biol *15*, 550. https://doi.org/10.1186/s13059-014-0550-8.

94. Li, H., and Durbin, R. (2010). Fast and accurate long-read alignment with Burrows–Wheeler transform. Bioinformatics *26*, 589–595. https://doi.org/10.1093/bioinformatics/btp698.

95. Diaz, A., Park, K., Lim, D.A., and Song, J.S. (2012). Normalization, bias correction, and peak calling for ChIP-seq. Statistical Applications in Genetics and Molecular Biology *11*. https://doi.org/10.1515/1544-6115.1750.

96. Ramírez, F., Ryan, D.P., Grüning, B., Bhardwaj, V., Kilpert, F., Richter, A.S., Heyne, S., Dündar, F., and Manke, T. (2016). deepTools2: a next generation web server for deep-sequencing data analysis. Nucleic Acids Res *44*, W160–W165. https://doi.org/10.1093/nar/gkw257.

97. Zhang, Y., Liu, T., Meyer, C.A., Eeckhoute, J., Johnson, D.S., Bernstein, B.E., Nusbaum, C., Myers, R.M., Brown, M., Li, W., et al. (2008). Model-based Analysis of ChIP-Seq (MACS). Genome Biol *9*, R137. https://doi.org/10.1186/gb-2008-9-9-r137.

STAR★METHODS

KEY RESOURCES TABLE

REAGENT or RESOURCE	SOURCE	IDENTIFIER
Antibodies		
anti-H3K9me2	Abcam	ab1220; RRID: AB_449854
anti-H3K9me3	Active Motif	CatNo.39161; RRID: AB_2532132
anti-H3K14ac	Abcam	ab52946; RRID: AB_880442
anti-H3	Abcam	ab1791; RRID: AB_302613
Chemicals, peptides, and recombinant proteins		
Dynabeads Protein A	Invitrogen	10002D
Formaldehyde	Electron Microscopy Sciences	15680
HygromycinB	GoldBio	H-270
ProteinaseK	Invitrogen	25530049
Phenol chloroform isoamyl alcohol	Sigma-Aldrich	77617
G-418 Sulfate	GoldBio	G-418
Mag-Bind Total Pure NGS	Omega	M1378
PVDF Blotting Membrane	GE Healthcare	10600022
EMM powder	Formedium	PMD0402
Yeast extract	Gibco	2911929
DNaseI	NEB	M0303
Phenol chloroform,acidic	VWR	E277
Nourseothricin Sulfate	GoldBio	96736-11-7
Blasticidin S Hydrochloride Powder	Research Products International	B12200-0.5
1-naphthaleneacetic acid	Sigma-Aldrich	N0640
Thiamine hydrochloride	Thermo Fisher	148990100
Critical commercial assays		
Superscript III Reverse Transcriptase	Invitrogen	18080085
SYBR Green	BioRad	172–5120
NEBNext Ultra II FS DNA Library Prep Kit for Illumina	NEB	E7805
NEB Next Multiplex Oligos	NEB	E6609
Quibit dsDNA HS assay kit	Thermo Fisher	Q32854
RNeasy Mini Kit	Qiagen	74104
Deposited data		
H3K9me2/H3K9me3ChIP-seq	This study	GEO: GSE235806
RNA-seq	This study	GEO: GSE235807
S.pombe strains	This study	Table S1
Oligonucleotides		
qRT-PCR,ChIP-qPCR	This study	Table S2
Software and algorithms		
Prism v9.4.1	GraphPad Software Inc.	https://www.graphpad.com/scientific-software/prism/
bwa v0.7.17-r1188	Wellcome Trust Sanger Institute	http://bio-bwa.sourceforge.net
R (version 4.0.2)	Cran.R	https://cran.r-project.org/
ggplot2	Cran.R	https://ggplot2.tidyverse.org/
Trimmomatic v 0.39	Max Planck Institute of Molecular Plant Physiology	http://www.usadellab.org/cms/? page=trimmomatic
RStudio (version 1.4.1106)	RStudio	https://www.rstudio.com/

(*Continued on next page*)

Continued

REAGENT or RESOURCE	SOURCE	IDENTIFIER
USeq v9.2.9	Utah Bioinformatics Shared Resource Center	https://useq.sourceforge.net
deeptools v3.5.1	Max Planck Institute	https://github.com/deeptools/deepTools/blob/ master/docs/content/about.rst
IGV v11.0.13	Broad Institute and the Regents of the University of California	https://software.broadinstitute.org/software/igv/
MACS2	N/A	https://github.com/macs3-project/MACS
samtools v1.6	Wellcome Trust Sanger Institute	http://samtools.sourceforge.net/
bedtools v2.27.1	University of Utah	https://bedtools.readthedocs.io/en/latest/
STAR	Dobin et al. 2013[89]	https://github.com/alexdobin/STAR

RESOURCE AVAILABILITY

Lead contact

Further information and requests for resources and reagents should be directed to and will be fulfilled by the lead contact, Kaushik Ragunathan (kaushikr@brandeis.edu).

Materials availability

All unique/stable reagents generated in this study are available from the lead contact without restriction.

Data and code availability

- ChIP-seq and RNA-seq data have been deposited at GEO and are publicly available as of the date of publication. ChIP-Seq accession number is GEO: GSE235806. RNA-Seq accession number is GEO: GSE235807.
- This paper does not report original code.
- Any additional information required to reanalyze the data reported in this paper is available from the lead contact upon request.

EXPERIMENTAL MODEL AND STUDY PARTICIPANT DETAILS

All *S. pombe* yeast strains used in this study are listed in Table S1. Strains were generated using either established methods for lithium acetate or electroporation transformations, or by meiotic crossing followed by tetrad dissection. All strains were genotyped using a colony PCR protocol. Plasmid constructs to create modified nmt81-Epe1-3xFlag-AID and nmt81-Mst2-3xFlag-AID inserts were constructed by modifying an existing pFA6a 3xflag AID IAA-17 degron kanMX6 plasmid. Full plasmids were made using ligation methods following PacI digestion to insert the nmt81 promoter. This insert repaired the PacI site, allowing for a second PacI digestion to insert the CDS for Epe1 or Mst2. EMMC was used as the base media for all cell culturing experiments, and all cultures were grown at 32C. For experiments involving sampling cultures over a time-course, a small volume of cells from each timepoint culture was used to nucleate the culture for the next timepoint in the appropriate media.

METHOD DETAILS

Cell culturing and growth quantification

For colony size quantification, seed cultures were grown overnight at 32C in EMMC in liquid media. Seed cultures were then used to nucleate fresh liquid cultures at a low starting OD (< 0.3 OD) and allowed to grow for about 6-8 hours. An equivalent number of cells were then diluted and plated on solid media, either EMMC or EMMC media supplemented with 15μM thiamine and 500μM NAA and spread with sterile glass beads. Plated cultures were grown at 32C, and pictures were taken at 3 and 5 days from plating on a Biorad ChemiDoc with white epifluorescence. For individual plate pictures, image colors are inverted to highlight cell colonies. Images were further analyzed in FIJI for trimming plate edges, identifying individual cell colonies, and quantifying colony number and size. To calculate percentage survival, we calculated colony count ratios between EMMC and EMMC media supplemented with 15μM thiamine and 500μM NAA after five days of growth.

Western blotting

To test time-dependent depletion of Epe1, cultures were seeded at a low OD (∼0.3) in liquid media EMMC or EMMC supplemented with 15μM thiamine and 500μM NAA. For later memory experiments that switched Epe1 expression, cells cultured for five days in 15μM thiamine and 500μM NAA were harvested and a portion of the culture was used to start a new overnight culture in EMMC. This EMMC culture was then both harvested after 24 hours and used to inoculate a new culture in 15μM thiamine and 500μM

NAA for a second time. That culture was then sampled after an additional 24 hours. All cultures were harvested by centrifuging 3-5 OD, decanting supernatant, and storing harvested pellets at -80C.

To extract protein for immunoblotting, cell pellets were processed using a standard TCA precipitation protocol. Pellets were washed with 1mL of ice cold water, then resuspended in 150uL of YEX buffer (1.85 M NaOH, 7.5% beta-mercaptoethanol). Resuspended pellets were incubated on ice for ten minutes, then 150uL of 50% TCA was mixed into each sample and incubated for ten minutes on ice. Samples were then centrifuged for 5 minutes at 13000 rpm at 4C, after which the supernatant was decanted. Pellets were then resuspended in SDS sample buffer (125mM TRB pH 6.8, 8M urea, 5% SDS, 20% glycerol, 5% BME) and centrifuged for 5 minutes at 13000 rpm at 4C. Samples were then run on an SDS page gel at 45 minutes at 200V. Stain-free imaging was performed on a Biorad ChemiDoc. Gel transfer was then performed on a Trans-Blot Turbo Transfer to a nitrocellulose membrane. Immunoblotting was performed by blocking the nitrocellulose membrane with 5% non-fat dry milk in Tris-buffered saline pH 7.5 with 0.1% Tween-20 (TBST) for about an hour. Blots were then incubated overnight with primary antibody at 4C, then washed with TBST three times and incubated with secondary antibody for an hour. Incubated blots were imaged using enhanced chemiluminescence on a Biorad ChemiDoc.

eVOLVER growth assay

Continuous culture experiments were performed in eVOLVER, designed and set up as previously described.[52] Two replicate cultures of each strain were grown in 25 mL of EMMC media at 32C. Growth was maintained in log phase using "turbidostat" mode to constrain optical density between 0.1 and 0.6. When cultures rise beyond the maximum OD, a dilution event is triggered, and growth rate is calculated for the duration since the previous dilution by fitting OD measurements to the exponential equation: $OD600 = (initial\ density) * e^{(growth\ rate) * (time)}$. Media condition changes were executed by spiking individual culture vials as well as the input EMMC media with a 1000x concentrated solution of thiamine + NAA in DMSO. Influx and efflux operations were manually triggered to flush untreated media from the lines.

To calculate the time derivative decrease in growth rate post-Epe1 depletion, first 60 hrs (2.5 days) after addition of thiamine and NAA were considered. Time derivatives of growth rate were calculated at each pair of consecutive growth rates with MATLAB's gradient function. A moving average with a sliding window of length 3 was applied to the time derivative of the growth rate, and the minimum of this moving average was found to be the minimum change in growth rate for each experiment vial. Subsequently, the average and standard deviation of the minimum change in growth rate was calculated across triplicate experiment vials.

qRT-PCR and RNA sequencing analysis

Cultures were grown in liquid culture containing either EMMC media or EMMC media supplemented with 15μM thiamine and 500μM NAA. For *mst2Δ epe1^{deg}* time points 0-120hrs, cells were cultured and harvested from eVOLVER. For memory RNA experiments, *mst2Δ epe1^{deg}* cells were grown in manually maintained incubated cultures. Cells were grown to 0.3-1.0 OD and harvested by centrifuging ~10mL of culture at 2000 rpm for 2 minutes. Cell pellets were washed once in distilled water, centrifuged at 5000 rpm for 30 seconds, and stored at -80C.

Stored pellets were thawed on ice for 5 minutes, then resuspended in 750uL TES buffer (0.01M Tris pH7.5, 0.01M EDTA, 0.5% SDS). 750uL acidic phenol chloroform was immediately added afterwards, samples were vortexed, and then incubated on a heat block at 65C. Samples were incubated for a total of 40 minutes, with 20 seconds of vortexing every 10 minutes. Afterwards, heated samples were placed on ice for 1 minute, shaken, and transferred to phase lock tubes. Phase lock tubes were centrifuged for 5 minutes at 13,000 rpm at 4C, and the aqueous phase was transferred to a clean Eppendorf tube and ethanol precipitated. Isolated nucleic acids were then treated with DNAse I at 37C for 10 minutes and cleaned up on Qiagen RNeasy Clean-Up columns. Purified total RNA was converted to cDNA by annealing reverse primers complementary to target genes and reverse transcribing with SuperScript III Reverse Transcriptase (Invitrogen). qRT-PCR was performed with SYBR Green dye on a CFX Opus 384 Real-Time PCR System. All qRT experiments were reproduced for at least three independently growth replicates.

Libraries were prepared and sequencing was performed commercially. Raw fastq files were evaluated using FastQC (v0.11.9) and trimmed using Trimmomatic (v0.39) and aligned to the ASM294v2 *S. pombe* reference genome using STAR (v2.7.8a) then indexed using samtools (v1.10).[90–92] Bam files were grouped by genotype replicate and differential expression analysis was performed through Defined Region Differential Seq in the open source USEQ program suite (v9.2.9) (http://useq.sourceforge.net).[93] The cutoff for significant differential expression of pairwise gene comparisons was defined as a P value of <0.01 (prior to phred transformation) after Benjamini and Hochberg multiple testing corrections. For principal component analysis, rlog counts were used to perform MDS analysis, and custom ggplot2 R scripts were used to generate scatterplot figures. Volcano plots were drawn using the ggplot2 library, and heatmaps were drawn using the pheatmap library, as well as the standard R library and functions. RNAseq heatmaps consist of genes that are differentially expressed for at least one indicated time point. Gene Ontology analysis was performed using the web-based tool AnGeLi with a p-value cutoff of < 0.01 with FDR correction for multiple testing and default settings Britton et al.[72] Raw and processed data are deposited in GEO under the accession number GEO: GSE235808.

Chromatin immunoprecipitation, ChIP-seq library preparation and analysis

Cultures were grown in liquid culture containing either EMMC media or EMMC media supplemented with 15μM thiamine and 500μM NAA in manually maintained incubated cultures. Cells were grown to mid-log phase (0.9-1.6 OD) and then harvested by fixation with 1% formaldehyde for 15 minutes then quenched with glycine for 5 minutes. Fixed cultures were then centrifugated, washed twice

with 1xTBS, and stored at -80C. To process samples, frozen pellets were thawed at RT for 5 minutes, then resuspended in 300 uL chip lysis buffer (50 mM HEPES-KOH, pH 7.5, 100 mM NaCl, 1 mM EDTA, 1% Triton X-100, 0.1% SDS, and protease inhibitors). Glass beads (500uL, 0.5mm) were added to each tube and cells were lysed by bead beating in an Omni Bead Ruptor at 3000 rpm × 30 s × 10 cycles. Ruptured cells were then collected by using a heated sterile needle to pierce the bottom of each tube, then collecting the lysate in a fresh tube via centrifugation. Lysate was then sonicated in a Q800R3 Sonicator to fragment sizes ranging from 100-500 base pairs. Sonicated lysate was then centrifuged at 13,000 rpm for 15 minutes at 4C, and the liquid portion was transferred to a new tube. Protein content was normalized using a Bradford assay. 25uL of each sample was reserved as input, to which 225uL 1xTE/1%SDS was added. Protein A Magnetic Dynabeads were preincubated with either Anti-H3K9me2 [Abcam, ab1220] or Anti-H3K9me3 [Active Motif, 39161] antibody. 30uL beads preincubated with 2ug antibody was added to 500uL cell lysate and incubated for 3 hours at 4C. Beads were held on a magnetic stand for subsequent washing cycles. For each wash cycle, cells were centrifuged at 1000 rpm for 1 minute at 4C, placed on the magnetic stand and allowed to settle, then liquid was removed by vacuum pipette. Then 1mL wash buffer was added and samples were rotated for 5 minutes per wash. Samples were washed three times with chip lysis buffer, then once with 1xTE. Samples were then eluted by suspending the beads in 100uL 1xTE/1%SDS for 5 minutes at 65C, then extracting liquid. A second elution was performed with 150uL 1xTE/0.67%SDS. Input and immunoprecipitated samples were then incubated overnight at 65C. We then added 60ug glycogen, 100ug proteinase K, 44uL of 5M LiCl, and 250uL of 1xTE was added to each sample and incubated at 55C for 1 hour. DNA was then extracted using phenol chloroform extraction, followed by ethanol precipitation. Ethanol precipitated pellets were resuspended in 100uL 10mM Tris pH 7.5 and 50mM NaCl. qPCR was performed with SYBR Green dye on a CFX Opus 384 Real-Time PCR System. All ChIP experiments were reproduced for at least two independently grown replicates.

Libraries were prepared following the standard protocol for the NEBNext Ultra II DNA Library Prep kit. Libraries of *mst2Δ epe1*^{deg} *gcn5Δ* cells were sequenced on an Illumina Miseq, and all other libraries were sequenced on an Illumina Nextseq instrument. Raw fastq reads were evaluated using FastQC (v0.11.9) and trimmed using Trimmomatic (v0.39).[90,91] Trimmed reads were aligned to the ASM294v2 *S.pombe* reference genome using the Burrows-Wheeler Aligner (v0.7.17) and bam files were further processed using samtools (v1.10).[92,94] Bedgraph coverage files were generated using deepTools (v3.5.1) and normalized IP against input in SES mode.[95,96] ChIP-seq H3K9me3 peaks were called using MACS2 with -g 12.57e6 in broad mode with a cutoff of 0.05.[97] Bedtools intersect (v2.27.1) was used to identify genes overlapping with identified peaks. Heatmaps were generated using deepTools (v3.5.1).[96] Specific peak histograms were generated using the SushiR package and custom R scripts. Raw and processed data are deposited in GEO under the accession number GSE235808.

QUANTIFICATION AND STATISTICAL ANALYSIS

Data quantification and statistical analysis was performed in Prism. Replicate number is indicated in corresponding figure legends. Error bars of qRT-PCR and ChIP-qPCR represent standard deviation.